Aus der Klinik für Neurologie
der Medizinischen Fakultät Charité – Universitätsmedizin Berlin

DISSERTATION

Injury-induced DNA methylome plasticity in the peripheral nervous system of the rat

zur Erlangung des akademischen Grades
Doctor medicinae (Dr. med.)

vorgelegt der Medizinischen Fakultät
Charité – Universitätsmedizin Berlin

von

Meike Gölzenleuchter

aus München

Datum der Promotion: 04.09.2015

Table of Contents

Abstract

Introduction: Recently, the dynamic characteristics of the adult methylome have been demonstrated in the central nervous system. Whether external stimuli can provoke DNA methylation changes in the peripheral nervous system has not been studied. The present work was based on the hypothesis that L5 spinal nerve injury induces DNA methylation changes in the L5 rat dorsal root ganglion (DRG). A rodent model of neuropathic pain, the Spinal Nerve Ligation (SNL) was employed to test this hypothesis.

Methods: Reduced representation bisulfite sequencing (RRBS) was used to analyze DNA methylation of eight rat DRGs (four controls, four SNL). This method makes it possible to profile DNA methylation on a genome-wide scale, at single-nucleotide resolution. First, DNA is digested with a methylation-insensitive restriction enzyme, yielding fragments that contain at least two cytosine-phosphate-guanine-dinucleotides (CpGs). Subsequently the fragments are bisulfite-treated, leading to the desamination of the unmethylated cytosines into uracils, without affecting the other bases. Finally the fragments are amplified, sequenced and aligned to the reference genome.

Results: Using an early time point of 24h post ligation this work reports widespread, highly significant ($p \leq 10^{-4}$) cytosine hyper- and hypomethylation in about 1% of the 1.4 million CpGs captured by RRBS. These CpGs were termed dynamically differentially methylated CpGs (dDMCs). The epigenetic remodeling occurred mainly outside of CpG islands. 56% of the observed changes were located in promoter or genic regions and mainly affected genes belonging to the axon guidance pathway ($p < 10^{-11}$). Consistent with emerging models relying on genome-wide methylation and RNA-sequencing analysis, variation of methylation was not tightly linked with variation of gene expression.

44% of the dynamically changed CpGs were detected outside of genes. These intergenic dDMCs occurred in clusters, with neighboring dDMCs varying in the same direction. The positions of these dDMCs were compared to intergenic, tissue-specific differentially methylated CpGs (tDMCs) of liver, spleen, L4 control DRG and muscle. Dynamic changes affected those intergenic CpGs that were different between tissues ($p < 10^{-15}$) and almost never the invariant portion of the methylome (those CpGs that were identical across all tissues). This result suggests a dichotomy of the intergenic

methylome in an invariant part—which remains stable across different tissues and conditions—and a plastic part that is more susceptible to alterations and encompasses CpG sites capable of responding to environmental changes such as nerve injury (dDMCs).

After joining juxtaposed hyper- or hypomethylated dDMCs into respective regions, a motif enrichment analysis was performed. The top enriched DNA motifs matched with binding motifs of transcription factors with important roles in PNS development, regeneration, and sensory dysfunction, supporting the possibility that DNA methylation contributes to gene regulation by altering the conformation of transcription factor binding sites.

Conclusion: This study demonstrates extensive methylome plasticity in the adult PNS providing a genome-wide account of epigenetics in pain. Future studies may address which of the cell types found in the DRG, such as specific groups of neurons or non-neuronal cells are affected by which aspect of the observed methylome remodeling.

Zusammenfassung

Einleitung: Die dynamischen Eigenschaften des adulten Methyloms wurden kürzlich im zentralen Nervensystem beschrieben. Ob äußere Reize auch die DNA-Methylierungsmuster des peripheren Nervensystems beeinflussen können, wurde bisher nicht untersucht. Die Hypothese der vorliegenden Arbeit war, dass eine periphere Nervenschädigung Methylierungsveränderungen der DNA im Spinalganglion L5 hervorrufen kann. Dies wurde anhand eines neuropathischen Schmerzmodells nach Spinalnervenligatur (SNL) bei Ratten untersucht.

Methodik: Mittels „Reduced representation bisulfite sequencing“ (RRBS) wurden die Methylome von acht Spinalganglien (vier Kontrollen, vier SNL) 24h nach SNL analysiert. RRBS ermöglicht die genomweite Untersuchung von DNA Methylierungen mit einer Auflösungsgenauigkeit einzelner Basenpaare. Dabei wird die DNA zuerst mittels eines Restriktionsenzyms in Fragmente geschnitten, die mindestens 2 Cytosin-phosphat-Guanin-Dinukleotide (CpGs) enthalten. Die nachfolgende Behandlung mit Bisulfit führt zur Desaminierung der unmethylierten Cytosinbasen in Uracilbasen, ohne die anderen Basen zu beeinflussen. Abschließend werden die DNA Fragmente amplifiziert, sequenziert und an das Referenzgenom angeglichen.

Ergebnisse: Es zeigten sich weitverbreitete, hoch signifikante ($p \leq 10^{-4}$) Cytosin Hyper- und Hypomethylierungen in etwa 1% der durch RRBS erfassten 1.4 Millionen CpGs. Diese wurden unter dem Begriff „Dynamisch differenziell methylierte CpGs“ (dDMCs) zusammengefasst. Die epigenetische Umgestaltung erfolgte größtenteils außerhalb der sogenannten CpG Inseln. 56% der beobachteten Veränderungen befanden sich in Promoter- oder Genregionen, insbesondere in Genen der „axonalen Wegfindung“ ($p < 10^{-11}$). Die vorliegende Arbeit fand keine Korrelation zwischen den Methylierungs-veränderungen und der Variation der Gen Expression und reiht sich damit in die wachsende Zahl von Studien mit genomweiten Analysen ein, die für eine komplexere Interaktion zwischen Methylom und Transkriptom sprechen.

Die anderen 44% der dynamisch veränderten CpG Methylierungsmuster befanden sich außerhalb von Genen. Diese intergenischen dDMCs traten in Clustern auf, wobei sich benachbarte dDMCs immer in die gleiche Richtung veränderten. Ihre Positionen wurden mit intergenischen Gewebe-spezifischen differenziell methylierten CpGs (tDMCs) von

Leber, Milz, Spinalganglion L4 und Skelettmuskel, verglichen. Bemerkenswert war, dass sich die Positionen der dDMCs mit denjenigen der tDMCs deckten ($p<10^{-15}$) und fast nie den invarianten Teil des Methyloms betrafen (diejenigen CpGs, die in allen Geweben identisch sind). Das intergenische Methylom lässt sich damit in zwei Teile gliedern: ein invarianter Teil – welcher zwischen unterschiedlichen Geweben und unter verschiedenen Bedingungen unverändert stabil bleibt – und ein plastischer Teil, der auf Umwelteinflüsse wie z.B. die Verletzung des Spinalnervs reagieren kann.

Weiterhin wurden die benachbarten hyper- oder hypomethylierten intergenischen dDMCs zu Regionen zusammengefügt und mittels Sequenzanalyse untersucht. Die häufigsten DNA Motive entsprachen Bindungsmotiven für Transkriptionsfaktoren mit wichtigen Rollen in der Entwicklung und Regeneration des peripheren Nervensystems und in sensorischen Funktionsstörungen. Methylomveränderungen könnten daher regulatorische Fernwirkungen auf Gene ausüben und so zur Entstehung, Aufrechterhaltung oder Regeneration neuropathischer Schmerzen beitragen.

Schlussfolgerung: Die vorliegende Arbeit weist die ausgedehnte Plastizität des Methyloms im adulten peripheren Nervensystem nach. In weiterführenden Studien muss untersucht werden, welche einzelnen Zelltypen des Spinalganglions von charakteristischen Veränderungen betroffen sind.

Index of abbreviations

A: adenine

bp: base pair

C: cytosine

CCI: chronic constriction injury

CGI: CpG island

ChIP-Seq: chromatin immunoprecipitation sequencing

CNS: central nervous system

CpG: cytosine-guanin-dinucleotide

DMC: differentially methylated CpG

dDMC: dynamically differentially methylated CpG

DNMT: DNA methyltransferase

DRG: dorsal root ganglion

G: guanine

GLM: generalized linear model

HCP: high-density CpG promoter

HOMER: hypergeometric optimization of motif enrichment algorithm

kb: kilobase

LCP: low-density CpG promoter

LRT: likelihood ratio test

NSA: non steroidal anti-inflammatory analgesics

PCR: polymerase chain reaction

PNS: peripheral nervous system

RPKM: reads per kilobase per million mapped reads

RRBS: reduced representation bisulfite sequencing

SNI: spared nerve injury

SNL: spinal nerve ligation

T: thymine

tDMC: tissue-specific differentially methylated CpG

tIMC: tissue-invariant methylated CpG

TSS: transcription start site

U: uracil

WGBS: whole-genome bisulfite sequencing

1 Introduction

1.1 Neuropathic pain – Definition and overview

Injury to the peripheral nervous system (PNS) is a clinical cause (and laboratory model) of chronic, neuropathic pain and, unless regeneration occurs, neurological debility. Neuropathic pain can originate from mechanical nerve lesion (e.g. due to surgery, amputation or tumor), neurotoxic chemotherapy (e.g. cisplatin), infectious disease (e.g. HIV, VZV), diabetes or neurological disorder (e.g. multiple sclerosis). The International Association for the Study of Pain (IASP) defined neuropathic pain as "Pain caused by a lesion or disease of the somatosensory nervous system" (IASP 2011). Neuropathic pain is characterized by (1) hyperalgesia, i.e. a diminished threshold to nociceptive stimuli (2) allodynia, i.e. pain in response to tactile, innocuous stimuli (3) spontaneous pain. Depending on the position of the lesion site, central and peripheral neuropathic pain can be differentiated. This work focuses exclusively on peripheral neuropathic pain, i.e. pain caused by a lesion or disease of the *peripheral* somatosensory nervous system.

PNS injury elicits a dynamic genome response in affected cells reflected in the alteration of hundreds of RNA transcripts in the dorsal root ganglion (DRG) in the rat [1–3]. Whether these changes are accompanied by epigenetic remodeling on a grand scale has not been meaningfully investigated to date, yet the involvement of DNA methylation has been discussed in that context (most recently by Denk and McMahon, 2012) [4].

It is estimated that between 1 and 18% of the population of Western Europe and North America suffers from neuropathic pain. However, depending on the study design and country under consideration the prevalence highly differs [5, 6]. Complete pain relief is rare and a reduction of the pain intensity by 30% is regarded as a good response [7].

1.2 Treatment of neuropathic pain

To date the treatment of neuropathic pain is principally symptomatic. Pharmacological approaches with non steroidal anti-inflammatory analgesics show only moderate effect [8, 9]. The European Federation of Neurological Societies Task Force guidelines [10] recommends tricyclic antidepressants (e.g. amitriptyline), serotonin and norepinephrine re-uptake inhibitors (e.g. duloxetine), voltage-gated calcium channel ligands such as gabapentin or pregabalin as well as topical lidocaine as 1st line treatment options for neuropathic pain. 2nd line treatment comprises tramadol and other

weak opioids. Due to their more severe side effects, strong opioids should be reserved for 3rd line treatment. Weak and strong opioids can be combined with 1st line medication. These recommendations are in agreement with other evidence-based guidelines like those of the International Association for the Study of Pain (IASP)/Neuropathic Pain Special Interest Group (NeuPSIG) [11]. In the majority of patients however, pain cannot be permanently relieved. Invasive therapy can then be considered. Interventions include the implantation of an epidural catheter, enabling drug delivery directly to the nerves, permanent nerve blocks with neurolytic agents or radiofrequency as well as electrical spinal cord stimulation. However, both conservative and invasive treatment can at best suppress patients' symptoms. They are unable to reverse the established painful state. This highlights the necessity to identify the initial mediators of neuropathic pain in order to develop new druggable targets acting directly on the source of PNS dysregulations. Only then will adequate pain management be achieved.

1.3 Mechanisms of neuropathic pain

1.3.1 Normal pain signaling

Painful stimuli such as heat, pressure or chemicals are converted into electrical impulses and transmitted from the skin to the dorsal horn via two types of afferent nociceptive fibers, the high-threshold Aδ- and C-fibers, that form parts of the spinal nerve. A particularity of these 1st order sensory neurons is that they are pseudounipolar, i.e. the cell bodies are located in the dorsal root ganglion (DRG) and project both to the periphery and to the spinal cord via one axon that bifurcates. Aδ nerve fibers are thinly myelinated and therefore faster conducting then the unmyelinated C-fibers (2-30m/s vs. 0.5-2m/s). Aδ-fibers are responsible for the transmission of acute, sharp pain stimuli, whereas C-fibers forward impulses perceived as burning, long lasting pain. The C-fibers synapse to 2nd order neurons in the Rexed lamina I and II (substantia gelatinosa) of the dorsal horn. These decussate to the contralateral side and ascend the spinal cord in the lateral spinothalamic tract. In the thalamus they form a synapse with 3rd order neurons which conduct the electrical impulse to the primary somatosensory cortex. There, the pain is finally perceived. By contrast, the Aδ-fibers separate into two branches when arriving in the spinal cord. One ascends directly to the thalamus, the other synapses to 2nd order neurons in Rexed laminae I, II and V. Figure 1 shows a section of a rat DRG. Morphologically two subtypes of sensory neurons can be distinguished, the large-

diameter and the small-diameter cell bodies. Large-diameter neurons can be attributed to the thinly-myelinated, fast conducting A-fibers, whereas the small-diameter neurons are part of the slow conducting C-fibers. The cell bodies of the sensory neurons are surrounded by satellite cells, glial cells with analogous roles as the astroglia in the central nervous system [12].

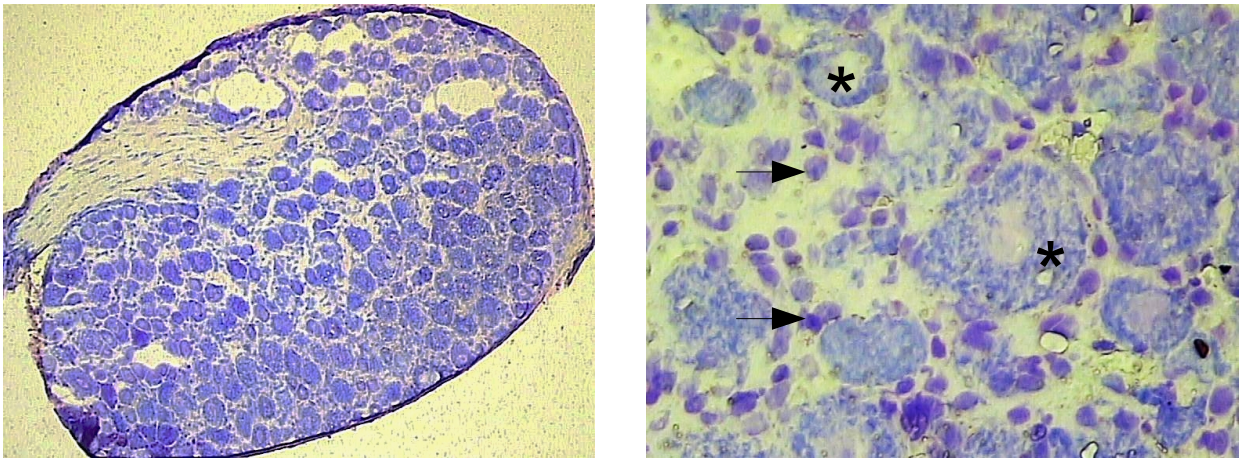

Figure 1: Configuration of the rat dorsal root ganglion at lumbar spinal nerve 5 level (L5 DRG). a. Global composition of the DRG visualized using a 10X objective. The cell bodies of the sensory neurons are stained violet. On the left side of the section the transition to the spinal nerve is shown. b. 100X objective. Sensory neurons (stars) are surrounded by satellite cells (arrows). Pictures were made by myself using the ArcturusXT™ laser-capture microdissection instrument.

1.3.2 Pathological pain

If the above mentioned pain signaling system is altered, acute pain—which has a physiological, protective function—can transform into chronic, neuropathic pain. This form of “pathological” pain results from a maladaptive plasticity of the PNS to injury and persists long after the primary nerve damage has healed. The mechanisms underlying this inaccurate remodeling have been the subject of intense research in the field but remain challenging to examine in humans, as anatomical structures like the dorsal root ganglions, which comprises the genetic information of the sensory neurons are difficult to access. This led to the development of different animal models in which the human neuropathic pain state is imitated by nerve injury. These procedures make it possible to analyse the anatomical structures involved in pain signaling *in vivo* or after sacrificing the animal and promote the understanding of the potentially similar processes

implicated in humans.

One characteristic of neuropathic pain is allodynia, i.e. the perception of normally innocuous stimuli as painful. This can be achieved by a threshold reduction of the nociceptive Aδ and C-fibers resulting in an increased excitability, leading to a "peripheral sensitization". The impulse transmission is further enhanced by additional synaptic connections in the dorsal horn, a process commonly termed “central sensitization” [13], which normally disappears as the lesion heals. Additionally, some studies suggest that after peripheral nerve injury the mechanical, low-threshold Aß-fibers establish connections with nociceptive 2nd order neurons in the superficial dorsal horn, which normally only receive impulses from Aδ and C-axons [14–17]. These mechanisms could explain why even a tactile stimulus of low intensity can create pain.

Moreover, it was shown that spinal nerve injury in the rat leads to ectopic electrical impulses not only in the axons of damaged sensory neurons but also in their somata located in the DRG, presumably causing spontaneous pain in the absence of noxious stimuli and contributing to pain chronification [18, 19]. Evidence exists that this ectopic activity expands to non-injured neighboring afferents after peripheral nerve lesion, possibly due to paracrine secretion from injured nerves acting on intact fibers [20].

But how are these changes orchestrated? And why does acute pain transform into a chronic condition in some patients and not in others? These questions still need to be fully elucidated in order to optimize patients' treatment. While a heritable component in pain susceptibility was identified in rodents and humans [21–23], genetics cannot explain the disparity of pain sensitivity in its entirety, as suggested by twin studies [24]. It is therefore likely that other mechanisms related to the individual's interaction with his environment—possibly mediated through epigenetic modifications—contribute to the reorganization of the PNS in response to nerve damage.

1.3.3 Gene expression in the dorsal root ganglion is altered after nerve injury in rodent models of neuropathic pain

In 2004 the rat genome was sequenced to over 90% by the Rat Genome Sequencing Consortium [25], opening the field for genomic studies in this species. In the rat, PNS injury elicits a dynamic genome response in affected cells reflected in the alteration of hundreds of RNA transcripts in the dorsal root ganglion (DRG) [1–3]. These gene

expression changes are of particular interest for the present work, as DNA methylation is thought to regulate transcription [26–29] and will therefore be detailed here.

Michaelevski et al. examined L4/L5 DRG (pooled samples) after crush lesion of the sciatic nerve and found widespread gene expression changes commencing 8h after injury and reaching a peak at the 18, 24 and 28h timepoints affecting 2700 genes (as compared to sham operated rats) [3]. Costigan et al. compared the gene expression profiles in L4/L5 DRG (pooled) between 3 commonly used rat models of neuropathy [1], i.e. spared nerve injury (SNI) [30], chronic constriction injury (CCI) [31] and spinal nerve ligation (SNL) [32]. Across the 3 models 1238 genes were altered, however only 124 were common to all. The majority (754 genes) were present only in the SNL model, which correlates with the severity of damage: Complete dissection of the L5 spinal nerve vs. partial dissection (SNI) or loose sciatic nerve ligations (CCI). In a study by Hammer et al., the authors performed L5 spinal nerve ligation and compared the anatomically intact L4 DRG between sham operated and SNL animals at a two weeks and two months timepoint [2]. About 2000 known protein-coding genes were found to be altered 2 weeks after SNL and the majority of these changes persisted after two months, suggesting that (1) the non-injured L4 DRG receives signals from the damaged sensory neurons of L5 (2) transcriptional reprogramming might contribute to the chronification of pain. Whether these transcriptional changes are accompanied by the remodeling of the epigenomic landscape remains unknown.

1.4 Epigenetics

1.4.1 Generalities about epigenetics and DNA methylation

The term "epigenetics" comprises processes that are epi- “above” genetics, i.e. not modifying the DNA sequence itself, yet heritable through cell division and required for the establishment and maintenance of cell-identity. The two main epigenetic mechanisms are histone alteration and DNA methylation. Both are thought to modify the accessibility of DNA by exposing or protecting the DNA from the cellular machinery. Thereby epigenetic mechanisms potentially influence the regulation of gene expression. The present study focuses on DNA methylation. The importance of DNA methylation has been highlighted by its role in X-chromosome inactivation in females [34], imprinting, i.e. parental specific methylation of one allele of a gene established during gametogenesis [35] and carcinogenesis [36, 37].

In somatic mammalian tissues, DNA methylation occurs almost exclusively at "CpG sites" (5'—cytosine-phosphate-guanine—3'), i.e. a cytosine preceding a guanine on the 5' to 3' end of one DNA strand. A methyl-group (—CH3) can be covalently attached to or removed from the 5-position of the cytosine by specific enzymes, the DNA methyltransferases (DNMTs). DNA methylation is seen in all regions of the genome and its different patterns demarcate the tissue specific "methylome" [38–40]. These tissue-specific epigenomic patterns seem to emerge from a genome-wide reprogramming of DNA methylation during mammalian embryogenesis [41, 42]. However, while organ differences—because they are stark and persistent—highlight the lifelong stability of the methylome, recent studies in the CNS have demonstrated dynamic modification of CpG sites in response to neural activity [43] akin to the remodeling of other chromatin marks, which can occur rapidly. These findings are in line with recent reports by others, revealing a previously under-appreciated role of DNA methylation in somatic, differentiated cells. Indeed, the involvement of epigenetic processes has been examined in a multitude of neurobiological processes such as memory formation [44], Alzheimer [45, 46], postnatal neurodevelopment and aging [47, 48].

1.4.2 CpG sites are unevenly distributed across the genome

While DNA methylation affects cytosines in a CpA context (cytosine-phosphate-adenosine) during development [42], in adult somatic tissues, methylation is confined to CpG sites. These sites are unevenly distributed across the genome, forming regions that are more or less rich in CpGs. Regions of high-CpG density are commonly named CpG islands (CGIs). They were first described by Gardiner and Frommer in 1987 and defined as regions ≥ 200bp with a G+C content greater than 50% and an observed to expected ratio of CpG ≥ 0.6 [49]. CGIs are often associated with promoters and usually unmethylated in normal tissues [50]. In the past, CpG islands were the main focus of methylation studies [40, 51–53]. However, emerging models found that methylation changes occur mostly outside of CGIs, in CpG poor regions, while CGIs remain largely stable through different conditions [54–59]. Regions surrounding CGIs termed "CpG island shores" seem to be targeted by methylation alterations in carcinogenesis and tissue differentiation [58, 60]. Additionally, in mammalians, genes can be dichotomized in low-CpG-density promoter genes (LCP genes) and high-CpG-density promoter genes (HCP genes) [56, 57] depending on the abundance of CpG sites in their promoter region

(see methods for details). CGIs obviously partially overlap with HCP, yet CGIs can also be found in intergenic regions, exons and introns. Promoters with a high-CpG-density (HCPs) are usually found to be poorly methylated [59, 61] and seem to be associated with house-keeping genes that are constitutively expressed in all cells and essential to maintain basal cellular functions [62]. LCP, by contrast, seem to represent regions which are more plastic [63, 64] and their role in differential gene expression is controversially discussed. Yet, the paradigm of promoter methylation resulting in gene silencing and vice-versa seems to be largely outdated.

1.4.3 Role of DNA methylation in the nervous system

The dynamic characteristics of epigenetic alterations in the nervous system have been described in recent studies. Guo et al. profiled the methylome of the mouse hippocampus after electroconvulsive stimulation and found that 1.4% of the 220,000 CpGs analyzed were differentially methylated as early as after four hours [43]. In another report, DNA methylation in different honeybee-phenotypes was studied [66]. The authors showed that subcaste switching from nurses to foragers was associated with methylation changes in honeybees' brains. The alterations could be reversed when the reverse transition to the nurse-phenotype was induced, underlining the aptitude of epigenetics for responding rapidly to environment. Miller et al. examined DNA methylation of calcineurin, a memory-associated gene, in the prefrontal cortex of rats and found that fear conditioning training triggered the hypermethylation of calcineurin within 24h [67]. Hypermethylation persisted at a later timepoint of 30 days, suggesting that DNA methylation plays a role in the establishment and maintenance of long-lasting memory. Klengel et al. found that individuals with a specific polymorphism in FKBP5 gene who experienced abuse in childhood were significantly more susceptible to develop psychiatric disorders in adulthood [68]. The authors suggested that in these risk-allele carriers, increased cortisol release following childhood trauma is associated with increased demethylation in glucocorticoid response elements of the FKBP5 gene and that this demethylation—when occurring during childhood—remains stable over time, making the individuals more susceptible to develop stress-related disorders such as posttraumatic stress disorder and depression in adulthood. These conclusions indicate that DNA methylation may be capable of encoding the effect of environmental factors on lifelong persisting behavioral traits in the neural genome.

Denk & McMahon suggested in a recent review article that "direct evidence that epigenetic mechanisms could be involved in the development and/or maintenance of chronic pain conditions is only just beginning to surface, and [that] the field is in its infancy"; [that] "the currently available data suggest that epigenetic mechanisms may be important contributors to chronic pain states"; and that "descriptive studies, for instance examination of genome-wide ... methylation in various models of chronic pain, will be useful [4]." Whether the neural genome is widely altered after PNS injury, such as by epigenetic remodeling, has not been determined but candidate gene studies suggest the possibility [69–72].

Zhang et al. studied histone acetylation in the brainstem in models of neuropathic and inflammatory pain in rodents. Persistent pain induced histone hypoacetylation at the Gad2 promoter in neurons of the nucleus raphe magnus, an important structure for central mechanisms of pain [69]. This epigenetic modification led to the suppression of Gad2 transcription, thereby decreasing GABA synaptic transmission, resulting in sensitized pain behavior. Using the rat model of chronic constriction injury (CCI), Zhu et al. observed elevated mRNA expression levels of the histone acetyltransferase p300 in the lumbar spinal cord [71]. Suppression of p300 was associated with diminished allodynia and thermal hyperalgesia and accompanied by decreased expression of COX-2, supporting the role of p300 in the epigenetic regulation of COX-2 expression and neuropathic pain. These findings are in line with a recent report by Uchida et al., where the (expected) upregulation of BDNF (brain-derived neurotrophic factor) one day after nerve injury in the mice DRG was accompanied by a notable increase in histone acetylation at its promoter [72]. While these reports focused on epigenetic alterations affecting histones, a few reports also indicate the potential role of DNA methylation in pain.

Tajerian et al. assessed the methylation status of the SPARC promoter in mice, a gene encoding for an extracellular matrix protein whose deficiency has been associated with disc degeneration and chronic back pain [70]. The authors observed that decreased SPARC expression in aging and SPARC-null mice correlated with increased methylation of the SPARC promoter in the lumbar discs. Intrathecal and intravenous administration of 5-azacytidine, a drug known to inhibit methylation [73], could partially reverse these changes, suggesting that DNA methylation is involved in the gene regulation of SPARC.

Recently, the same authors investigated global methylation in different regions of the mouse brain following spared nerve injury [74]. Using the luminometric methylation assay (LUMA), a method to estimate global methylation, they observed decreased global methylation of ~10% in both the prefrontal cortex and the amygdala six month after peripheral nerve injury. Yet, this long-lasting, central epigenetic remodeling could be influenced by environmental enrichment (running wheel, marbles etc) emphasizing the dynamic characteristics of the methylome.

1.4.4 Assessment of genome-wide DNA methylation - Reduced representation bisulfite sequencing (RRBS)

Sequencing technologies have opened the door to genome-scale DNA methylation analysis at single base-pair resolution. Bisulfite sequencing has become a widely used method for mapping DNA methylation [56, 64, 75, 76]. It can be performed as whole-genome shot gun or reduced representation bisulfite sequencing (RRBS). Bisulfite sequencing yields digital data for each CpG, a count of reads indicating “methylated” and a count of reads indicating “unmethylated.” RRBS was developed in 2005 [77] and its improved version has become the technology of choice for genome-scale DNA methylation profiling. In contrast to array-based techniques, bisulfite sequencing does not preselect genomic regions of interest such as promoters, yet provides a genome-wide methylation map, including intergenic regions, introns and exons.

1.5 Rat model of neuropathic pain - L5 spinal nerve ligation model

To study peripheral neuropathic pain in humans—from the mechanisms underlying its establishment to its course and chronification—it is necessary to create laboratory models that are reproducible, testable and provide the best analogy to human pain behavior. Such a model was introduced by Chung et al. in 1992 [32] and is illustrated in Figure 2. The “spinal segmental nerve ligation” (SNL) consists of ligating and cutting the L5 spinal nerve distal to its corresponding dorsal root ganglion (DRG) in the rat. The L5 spinal nerve, along with the L4 spinal nerve, conducts the majority of the sensory afferents from the hindlimb. Chung et al. observed that the L5 SNL causes long-lasting mechanical allodynia and hyperalgesia to heat when the hind paw of the operated side is stimulated. To quantify the mechanical allodynia, von Frey monofilaments of increasing forces are applied to the plantar side of the ipsilateral paw and the withdrawal frequencies are compared to those of control animals. In operated rats,

innocuous tactile stimuli (no paw withdrawal in controls) induce paw lifting. Similarly, the latency of hindlimb withdrawal in response to noxious heat stimulation of the affected side is decreased in operated rats. Thereby the SNL model resembles peripheral neuropathic pain in humans. By means of behavioral testing the success of the surgery can be visualized and objectified. Furthermore, unlike models which damage the sciatic nerve, the L5 SNL model allows for a distinct analysis of the cell bodies of the injured L5 DRG neurons and the intact L4 DRG neurons. It became a well-proven model for neuropathic pain in the rat and has been widely used [18, 56, 78–80]

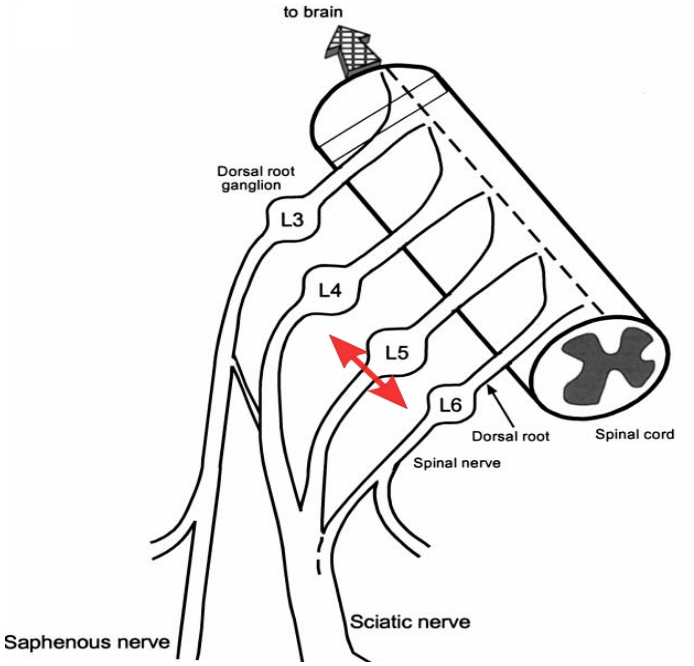

Figure 2: Schematic representation of the L5 spinal nerve ligation (SNL) procedure and anatomical structures neighboring the L5 DRG. The red arrow represents the anatomical position of the nerve transection. Modified according to I. Decosterd, J.C. Woolf / Pain 87 (2000) 149-158

In humans, neuropathic pain is responsive to drugs like tricyclic antidepressants, gabapentin and opioids, while NSAs show very limited success. A report studying the pharmacological effects of these compounds in the L5 SNL rat model demonstrated that amitriptyline, gabapentin and morphine could partially or completely reverse tactile allodynia induced by SNL. By contrast, treatment with indomethacin remained ineffective [81]. These analogous conclusions between human and rat further support

the employment of the L5 SNL model as a reasonable animal model of peripheral neuropathic pain.

It is worth noting that nerve damage distal to the DRG (such as spinal nerve ligation and axotomy) must not be confounded with dorsal rhizotomy, where the dissection is performed proximally to the DRG on the nerve root. Paradoxically, while rhizotomy alleviates symptoms and is a neurosurgical procedure occasionally used in patients with a chronic pain condition, axotomy does not relieve the pain syndrome—quite the opposite—it constitutes its origin [82].

2 Aims and hypothesis

The main hypothesis of this work was that nerve injury can induce methylome alterations in the rat dorsal root ganglion. To analyze the plasticity of the neural rat methylome reduced representation bisulfite sequencing (RRBS) was used for genome-wide, quantitative comparisons of methylation levels at single nucleotide resolution.

In detail, this work poses the following questions:

- Can we observe genome-wide DNA methylation changes in the peripheral nervous system as early as 24h after peripheral nerve injury?
- Do the differentially methylated CpGs occur in neural-specific genes?
- Are DNA methylation changes tightly linked to gene expression changes?
- Do the differentially methylated CpGs located in intergenic regions have a particular role?
- Can the rat methylome be dichotomized in a plastic and an invariant part?

3 Materials and methods

3.1 Characteristics of the rat genome

The rat genome comprises 2.72 Gb (RGSC3.4), that are distributed on 22 chromosomes. This genome size is smaller that the human genome (2.9 Gb). It has been sequenced to ~ 95 % by the Rat Genome Sequencing Consortium [25] and encompasses 22,938 protein-coding genes (RGSC3.4). For genomic studies, the inbred rat strain of the *Rattus norvegicus* (Brown-Norway rat) is particularly well suited, as genetic polymorphism is substantially reduced.

3.2 Animal experiments and tissue procurement

Male Brown-Norway rats were used for all experiments. This strain was chosen because it is the reference strain of the publicly available *Rattus norvegicus* reference genome. None of the animals had a previous history such as prior drug administration, surgery, behavioral testing or other. All procedures involving live animals were reviewed and approved by the Institutional Animal Care and Use Committee (IACUC).

Rats were purchased from Charles River Laboratories and housed two per cage prior to the start of the experiment. Animals had a body weight of 250-300g. Before starting the experiments all animals got at least one week to familiarize themselves with their environment. All experiments and tissue harvesting were performed during the dark cycle of a 24 hour period. L5 spinal nerve ligation (SNL) was used as a rat model for peripheral nerve injury and performed as described by Chung et al. [32, 83]. In brief, L5 SNL was performed under deep anesthesia achieved through isoflurane inhalation. L5 SNL consisted of ligation of the left spinal nerve immediately distally to the L5 dorsal root ganglion (DRG) followed by cutting the nerve distally to the ligature. Control animals in the present study underwent isoflurane anesthesia and a skin incision followed by surgical wound closure without L5 SNL.

L5 DRG for analysis of dDMC analysis (by RRBS) were harvested 24h after the L5 SNL or the skin incision control procedure. L4 DRG; liver; skeletal muscle; and spleen for organism-wide identification of tDMCs and tIMCs (by RRBS) were harvested from animals sacrificed without a prior procedure. All DRG or other tissues were flash-frozen and stored at -80ºC.

Group sizes were n=4 for the SNL group and n=4 for the control group in the experiment determining DNA methylation levels. The group size was chosen based on the previous study characterizing the DRG methylome in control animals [56], which had demonstrated that RRBS of the DRG could be performed highly reproducibly by rigorously standardizing procedures for tissue procurement and library construction. The minimum group size of the experimental design matched the resource intensity of RRBS and the multiple strengths of the technology: reproducibility; genome-wide reach; single CpG resolution; and methylation level quantification from digital data (read counts), which can be analyzed by tests with high statistical power.

Characterization of organ specific methylomes (L4 DRG; liver; skeletal muscle; and spleen) were performed for each tissue in duplicate (n=2). This design was based on successful organ comparisons in recent reports by others [84] and further justified by the marked organ differences detectable by a hierarchical clustering analysis (Figure 17).

3.3 DNA extraction of the L5 DRGs and other tissues

DNA was extracted following the QIAmp DNA Micro Kit Protocol from Qiagen for isolation of genomic DNA from less than 10 mg of tissue. Briefly, the DRG was transferred in a 1.5 ml microcentrifuge tube,180 µl buffer ATL were added, followed by 20 µl of proteinase K. The mixture was pulsed-vortex for 15s. The microcentrifuge tube was then incubated at 56°C overnight in a thermomixer until the DRG was fully lysed. The next morning, 200 µl buffer AL was added and the mixture was vortexed immediately. Then 200 µl of ethanol (100%) was added, the mixture was immediately vortexed for 15s and incubated for 5min at room temperature. The lysate was transferred into a QIAmp MinElute column and centrifuged at 14,000 rpm for 1 min. The column was then placed in a new, clean 2 ml collection tube and the collection tube containing the flow-through was discarded. 500 µl buffer AW1 (washing buffer) was added to the column and centrifuged at 14,000 rpm for 1 min. The column was placed in a new, clean 2 ml collection tube and the collection tube containing the flow-through was discarded. The same step was repeated with 500 µl of buffer AW2. A 3 min centrifugation step (14,000 rpm) was added to dry the membrane completely. The QIAmp MinElute column was placed in a clean 1.5 ml microcentrifuge tube and 200 µl buffer AE (elution buffer) was added to the center of the membrane. After 5 min of incubation at room temperature, the column (in the 1.5 ml microcentrifuge tube) was

centrifuged at 14,000 rpm for 1 min. The column was discarded and the microcentrifuge tube containing the eluted DNA was kept for subsequent analysis.

NanoDrop 1000 spectrophotometer (Thermo Scientific) was used for quality control to ensure that the eluted DNA was free from contaminants. Qubit® 2.0 Fluorometer (Invitrogen) was used to determine the quantity of DNA that was eluted. One DRG yielded 1-1.5 µg of DNA.

A similar procedure was used for DNA extraction of spleen, liver, L4 DRG and skeletal muscle.

3.4 Reduced representation bisulfite sequencing (RRBS)

Bisulfite treatment of DNA leads to the desamination of cytosines (C) into uracils (U), without affecting the other bases. Following PCR amplification, Us are then converted into Ts. It is worth noting that methylated cytosines (^{m}C) also remain unaffected by this transformation, making it possible to bioinformatically retrace which cytosine was originally methylated and which not. The procedure is illustrated in Figure 3.

RRBS libraries were constructed with the EZ DNA Methylation Kit (Zymo Research) following the manufacturer's instructions. In brief, 250 ng of genomic DNA from each sample were digested with 200 U of MspI, a methylation insensitive restriction enzyme. DNA fragments were purified. Sticky ends resulting from the restriction digest were converted to blunt ends by end-repair using T4 DNA polymerase and Klenow enzyme (NEB). An 'A' nucleotide was added to the 3'-end of the blunted fragments and distinct adaptor sequences were ligated at both ends of the DNA fragments. Fragments between 30 and 300 bp were selected and gel-extracted. Libraries were then bisulfite-treated using the EZ DNA Methylation Kit (Zymo Research) following the manufacturer's instructions. Subsequently, samples were subjected to 15 cycles of PCR amplification. The amplification products were purified with Ampure XP magnetic beads. The resulting libraries were quality controlled and quantified on an Agilent 2100 micofluidic analyzer. Sequencing was performed on an Illumina HiSeq 2000 platform genome analyzer for 51 cycles in paired-end mode (2x51bp).

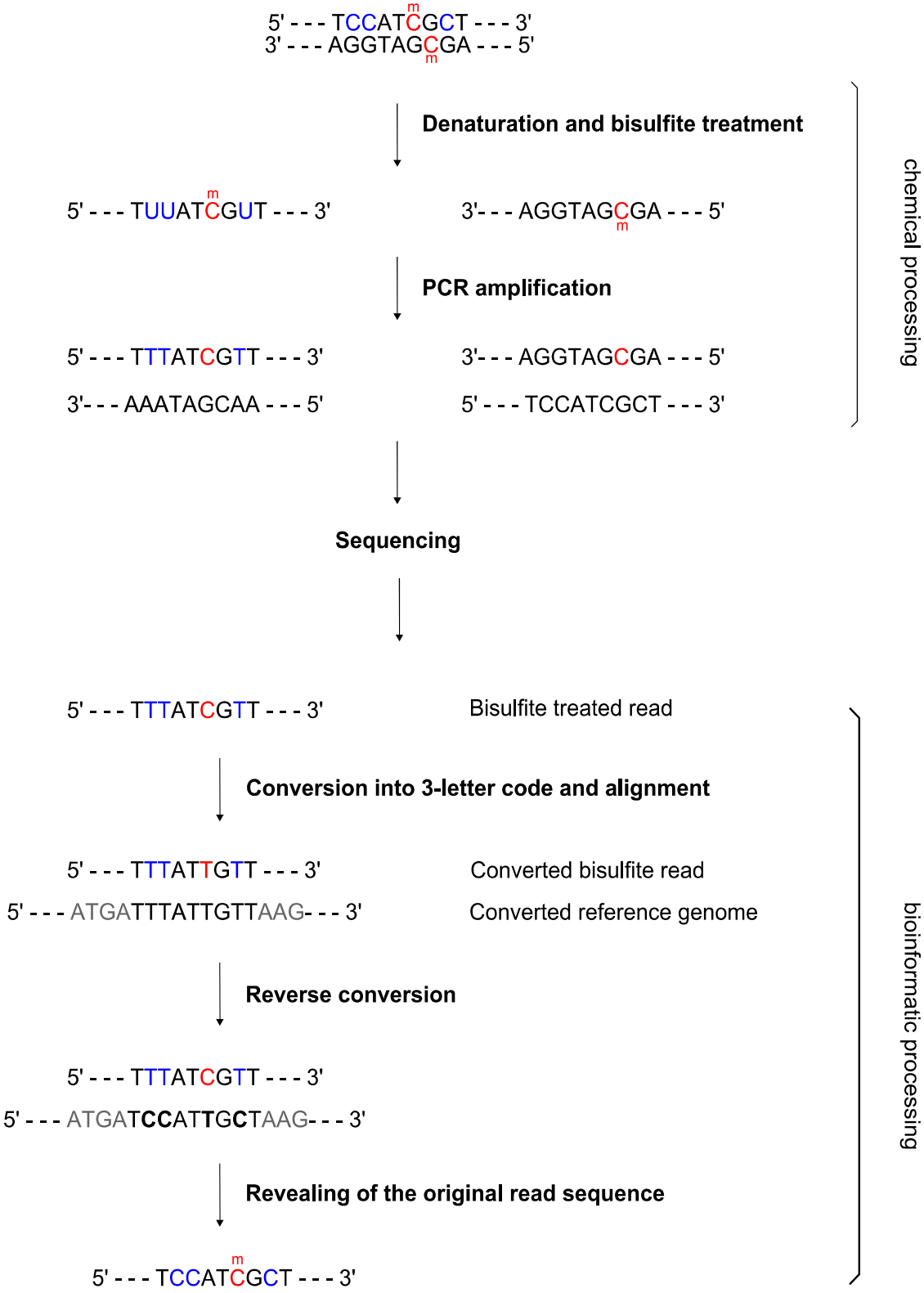

Figure 3: Mechanism of RRBS and read processing. The MspI digested DNA reads are denatured and bisulfite treated. Thereby unmethylated cytosines (C) are converted to uracils (U).The fragments are amplified by PCR. During this step uracils are further transformed into thymines. Methylated cytosines (mC) are converted into Cs. At the end

of PCR, all Cs originated from mCs. The reads obtained are subsequently sequenced. As the bisulfite treated DNA fragments diverge from their original sequence, they cannot align to the reference rat genome. It is necessary to bioinformatically convert both the RRBS-reads and the reference genome to a 3-letter-code (T,G,A) in order to correctly align both. Once aligned, both sequences are converted back to the 4-letter code (T,G,A,C), the mismatches revealing the original sequence of the DNA fragment.

3.5 Bioinformatic alignment of the RRBS reads to the rat genome

After removal of the adaptor sequences, the RRBS reads were mapped in the three-nucleotide space (A, G, T) to MspI fragments (30-300 bp length) predicted from the forward and reverse strand of the rat reference genome (rn4) using Bowtie2 [85] allowing for a maximum of two mismatches and retaining only uniquely aligning reads. Methylation levels were then determined as previously described [56] for all cytosines occurring within a CpG dinucleotide motif in the rat genome by computing the fraction of cytosines that was chemically protected from bisulfite conversion to uracil. A minimum coverage of ≥10 reads was required for each library to declare a methylation level; CpG sites covered by fewer reads in any of the replicates were excluded from subsequent analyses. Subsequently, in order to make a comparison between the different replicates/conditions/samples possible, only CpGs common to all samples were kept.

The bisulfite conversion rate, an important quality control parameter of RRBS experiments, was determined by computing the conversion rate of cytosines to uracil occurring outside of CpG motifs, where DNA methylation is expected to be absent and therefore bisulfite conversion of cytosines to uracils complete. Sequencing libraries were only accepted for downstream analysis if the bisulfite conversion rate was found to be ≥ 99%, thereby assuring that the fraction of unmethylated CpG could be underestimated in the present study only by <1%.

3.6 Annotation of CpG sites

The gene annotation Ensembl68 of the rat reference genome assembly version rn4 was used to assign CpGs into the bins “promoter”, “exon”, “intron” and “intergenic”. The promoter region of a gene was defined as a 2 kb window centered on the TSS. According to their CpG content we further defined high-density CpG promoter (HCP)

genes as genes with a promoter-CpG-content of ≥ 3.2% and low-density CpG promoter (LCP) genes, as genes with a promoter-CpG-content of < 3.2% [56]. This definition was adopted from the classification of human promoters by Saxonov et al. [57]. Similarly to the human genome, the promoter CpG density in the rat genome follows a bimodal distribution, which allowed dichotomization of promoters into two classes, HCP and LCP, with a cutoff at the inter-peak minimum [56].

Integrated Genomics Viewer (IGV, Broad Institute) was used to verify the correct assignment of CpGs to their respective genomic position.

Independently, CpGs were classified according to their localization within a CpG island (CGI) or a CpG island shore. CGIs were defined according to the UCSC genome browser as regions ≥ 200 bp with a G+C content greater than 50% and an observed-to-expected ratio of CpG ≥ 0.6 [49]. CpG island shores were defined as regions located within 2 kb of CpG islands [58]. Overlapping shores were merged into a single shore.

3.7 Calculation of methylation levels

RRBS yields digital data for each CpG, i.e. a count of reads indicating “methylated“ or “unmethylated“. The methylation status of a CpG is calculated as follows: (methylated reads)/(unmethylated reads + methylated reads). A value between 0 and 1 is obtained for each CpG (see Figure 4).

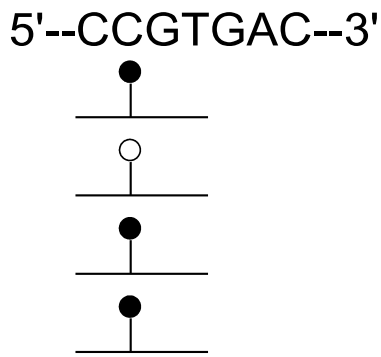

Figure 4: Calculation of methylation levels. In this example 4 reads were obtained for a CpG in a particular genomic position. Three reads are methylated (black) and one read is unmethylated (white), the methylation level is 0.75. However, such a CpG would not pass the quality criteria of the present work, as a minimum coverage of 10 reads for each CpG was required.

3.8 Clustering analysis of the L5 DRG CpGs

CpG sites were included if they were covered by ≥10 RRBS reads in each sample. For each CpG assessed by RRBS, a methylation level was computed. Then the Manhattan distance was calculated, corresponding to the sum of the pairwise, absolute difference between the methylation levels for each particular CpG position across the 8 samples. This procedure was repeated for all CpGs. Ward's method was applied for hierarchical clustering and yielded the dendrogram (Figure 7). The calculation was executed in R using the following command: hclust(dist(t(methylation_data_matrix), method = 'manhattan'), method = 'ward');

3.9 Statistical testing of individual CpG sites: dDMCs, tDMCs, and tIMCs

Each read can be either fully methylated or unmethylated for an individual CpG, following a binomial distribution. To test for differences in methylation at individual CpG sites, either between conditions (SNL vs. control, 1st experimental dataset) or between multiple tissues (liver, muscle, L4 control DRG, spleen, 2nd experimental dataset), each site was treated as a separate logistic regression. A generalized linear model (GLM) using a logistic link function was employed. The resultant likelihood ratio test (LRT) uses the binomial distribution of the raw counts directly and thus correctly calibrates the p-value between sites with high or low depth of coverage. The p-values of the LRT can be calculated using a chi-squared distribution. The deviance (difference between the observed and the expected model) obtained from the LRT test follows an approximate chi-squared distribution with one degree of freedom when considering the control vs. SNL condition and with three degrees of freedom when comparing muscle, spleen, liver and L4 DRG. For the control vs. SNL condition (dDMCs) a deviance value of 15 corresponds to a p-value $\leq 10^{-4}$. This significance level and an additional minimum absolute methylation difference of 0.08 between the two conditions was required to determine dDMCs. For the analysis of tissue-specific differentially-methylated CpGs (tDMCs), samples of liver, spleen, muscle and L4 DRG were considered. A similar significance level of $p \leq 10^{-4}$ was required (corresponding to a deviance ≥ 22) to declare a CpG as being a tDMC. The remaining CpGs were defined as invariant (tIMCs). To accurately compare the genomic position of tDMCs and dDMCs, the common CpGs between the two experimental datasets that were covered by ≥ 10 reads in all samples were considered.

3.10 Integrated analysis of dDMCs located in genes

Ingenuity Systems pathway analysis IPA was used for pathway analysis on differentially methylated genes defined by containing dDMCs in the promoter (2 kb centered around the transcription start site) or gene body. The Ingenuity IPA system was accessed through the website interface, the only currently available user interface http://www.ingenuity.com. The Ensembl IDs of genes were imported into IPA; a core analysis was conducted to identify the most enriched pathways; the list of differentially methylated genes occurring in the most significantly altered pathway, axon guidance, was downloaded and provided as Table 2; core pathway components were also represented graphically (Figure 11).

3.11 Distribution of dDMCs across gene deserts

Gene deserts (intergenic regions) differ in size. To analyze the distribution of dDMCs across gene deserts for the entire dataset, gene desert sizes were standardized to a length of 1. The span was then subdivided into 10 bins corresponding to an interval between percentile ranks as indicated in Figure 15. The frequency of dDMCs in each bin relative to the number of assayed CpG sites in the bin was then computed.

3.12 Clustering analysis of the tissue sample CpGs

Hierarchical clustering of the intergenic CpGs of liver, spleen, L4 DRG and muscle was performed using the same method as described above for the hierarchical clustering of the L5 DRGs and yielded the dendrogram represented by Figure 17.

3.13 Motif enrichment analysis comparing plastic and invariant deserts

A transcription factor motif enrichment analysis comparing plastic and invariant deserts was performed. Plastic deserts were formed by joining juxtaposed intergenic hyper- or hypomethylated dDMCs into respective regions using a sliding window of 100bp size. Invariant deserts were formed by applying the same procedure to intergenic tIMCs. Comparisons between plastic and invariant desert regions were then made for 301bp regions centered around each desert's interval midpoint. The window size and the demarcation of regions to be compared were chosen following the motif enrichment analysis methodology used by Ng et al. [54]. Enrichment analysis was then executed using the hypergeometric optimization of motif enrichment algorithm (HOMER) [86] version 4.2 (downloaded January 2013). Two comparisons were made: First

hypermethylated deserts (foreground) against invariant deserts (background); second, hypomethylated deserts (foreground) against invariant deserts (background).

3.14 Gene expression analysis

L5 DRG for the primary transcriptome analysis were harvested 24h after the L5 SNL or skin incision. Two biological replicates were available per condition. RNA isolation was performed using the TRIzol Reagent (Invitrogen) according to the manufacturer's protocol. For library construction the protocol for TruSeq RNA Sample Prep Kit v2 was followed. RNA-seq was performed on an Illumina HiSeq 2000 platform and the 50bp long reads were aligned to the rat genome (RGSC v3.4) by the Bowtie 2 algorithm. Reads with more than two mismatches were discarded and only uniquely mapped reads were kept. ENSEMBL genome browser 67 was used to annotate the genes. A coverage ≥ 20 reads in each replicate of either the control or the SNL condition was required, resulting in 10,315 genes. To normalize for the total read length and the number of sequencing reads, RPKM (Reads Per Kilobase per Million mapped reads) was applied to each read [87]; First, a pseudo-count of 1 was added to each exon, then RPKM was applied and the RPKM values were $\log_2$-transformed. Genes with a [$\log_2$ (fold change)] of ≥ 0.6 or ≤ -0.6 were defined as dysregulated (corresponding to a fold change of ≤ -1.5 or ≥1.5).

3.15 Database administration and management

MySQL Workbench was used to manage methylation- and gene expression data. For methylation data, information of each of the 1.4 million assessed CpGs (rows) was gathered in 21 columns. The columns comprised the chromosome number, strand, position on chromosome, context (CGC, CGA, CGT or CGG), position relative to genomic features (inside or outside of promoter, exon, intron, intergenic region, CGI, CGI shore, HCP, LCP), RefSeq name, Ensembl name, deviance, methylation difference and the raw methylation levels for that CpG in each of the four control and four SNL DRGs. For expression analysis, each row corresponded to a gene. The 16 columns contained the Ensembl gene name, RefSeq gene name, chromosome number, strand, genomic position of gene begin and end, numbers of CpGs in the gene, CpG content in promoter (LCP or HCP gene), raw read counts and RPKM values for both control and both SNL DRGs and the $\log_2$(RPKM) value.

4 Results

4.1 Genome-wide quantification of CpG methylation by RRBS

The plasticity of the PNS methylome was tested by performing an L5 spinal nerve ligation (SNL), a common model of PNS injury and neuropathic pain [32] determining the methylation level at ~ $1.4x10^6$ CpG sites in the L5 DRG with reduced representation bisulfite sequencing (RRBS), a current technology providing digital quantification of CpG methylation levels. Figure 5 illustrates the different steps performed.

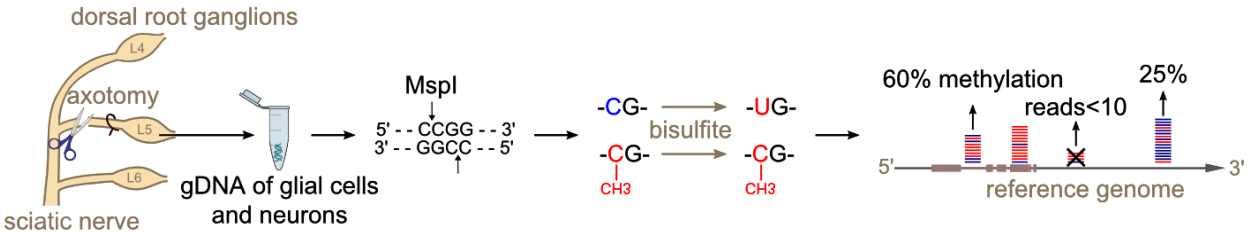

Figure 5: Experimental design. Genomic DNA from the L5 dorsal root ganglion (DRG) of Brown Norway rats was isolated 24h after spinal nerve ligation (SNL) or a sham procedure (negative control). Genomic DNA (gDNA) was isolated and subjected to a restriction digest with MspI. DNA fragments were ligated to adapter; bisulfite treated converting unmethylated cytosines to uracils; and sequenced. Resulting paired-end reads—1.1 billion in total from eight independent libraries analyzed in the present study—were aligned to the rat genome. Cytosine methylation levels were called only for CpG sites covered in a given library by ≥ 10 independent sequence reads.

The 1.4 million common CpGs between the 4 control and the 4 SNL DRG samples corresponded to 3% of all the CpG sites of the rat genome (see Table 1) and were distributed genome-wide, as shown by Figure 6.

	CpG sites in the rat genome	MspI sites (CCGG sites)	RRBS-captured CpG sites ≥ 10 reads
total	47,864,232	3,328,020	1,422,708
% of total CpG sites	100%	7%	3%

Table 1: Overview of the CpG sites in the rat genome

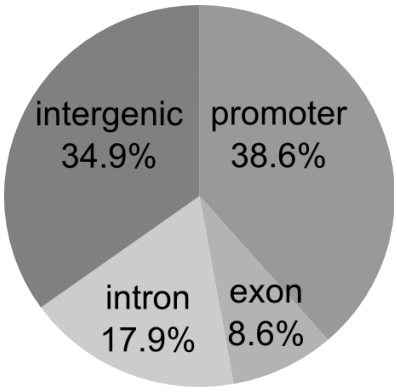

Figure 6: Genome-wide distribution of the captured CpGs. About 2/3 of the CpGs captured by RRBS were located in regions associated to genes (promoter, exon, intron). The boundaries between the promoter region and especially the 1st exon of a gene are imprecise, which explains the disparity between the CpG distribution in the promoters (38.6%) and exons (8.6%), as all CpGs overlapping a promoter and another feature were assigned to the promoter in the present study.

4.2 Nerve injury induces genome-wide methylation changes in the dorsal root ganglion

To determine whether nerve injury can induce any apparent methylation changes, a hierarchical clustering analysis was performed. All 1.4 million CpGs were included regardless of any significance level or magnitude of change in order to get the most global overview. The resulting dendrogram clearly separates two groups according to the two experimental conditions (Figure 7), suggesting systematic methylation alterations that are characteristic of spinal nerve injury.

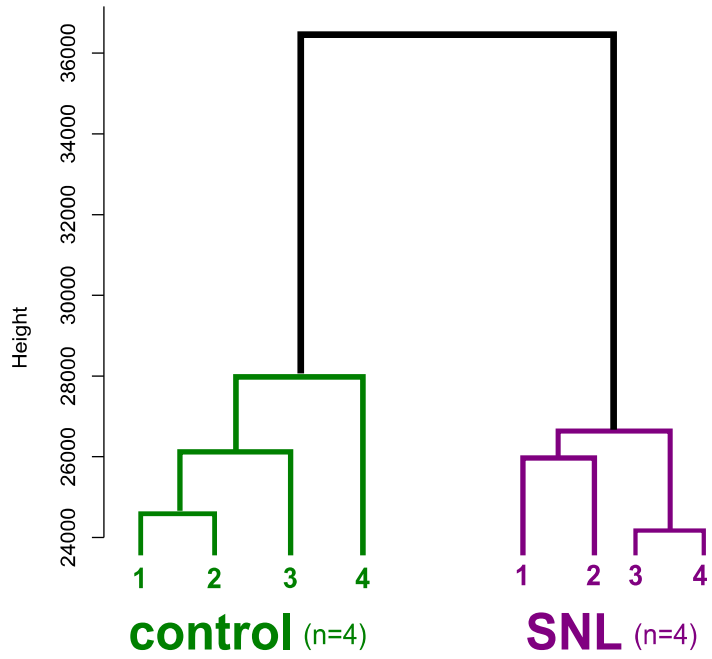

Figure 7: Nerve injury eliciting methylome alterations: Evidence at whole dataset level. DNA methylation was markedly altered after spinal nerve ligation. Hierarchical clustering—using all methylation levels measured at 1,422,708 CpG sites—clearly separated control animals (left) from SNL animals (right).

This initial result prompted us to examine the observed DNA methylation changes in greater detail. To test whether the alterations were statistically significant, the methylated and non-methylated reads from the SNL and control samples were fitted using a logistic regression model, i.e. a generalized linear model (GLM). A deviance exceeding 15 was considered as the critical threshold to declare that a CpG was differentially methylated following SNL. To increase the specificity, an absolute methylation change at each CpG site exceeding 8% was further required. The corresponding volcano plot is shown in Figure 8. Overall, very similar methylation patterns between the two conditions were observed. However, 14,965 CpGs were found to be highly significantly altered between SNL and controls ($p \leq 10^{-4}$), which corresponds to ~ 1% of all CpGs captured by RRBS. Interestingly, the majority (80%) were hypermethylated following spinal nerve ligation, while only 20% of the CpGs lost methylation. These dynamically altered CpGs occurred genome-wide, affecting both genic and intergenic regions and were termed “dDMCs—dynamically differentially methylated CpGs”, as they represent the response of the peripheral nervous system to

nerve injury. The distribution of these dDMCs is resumed in Figure 9.

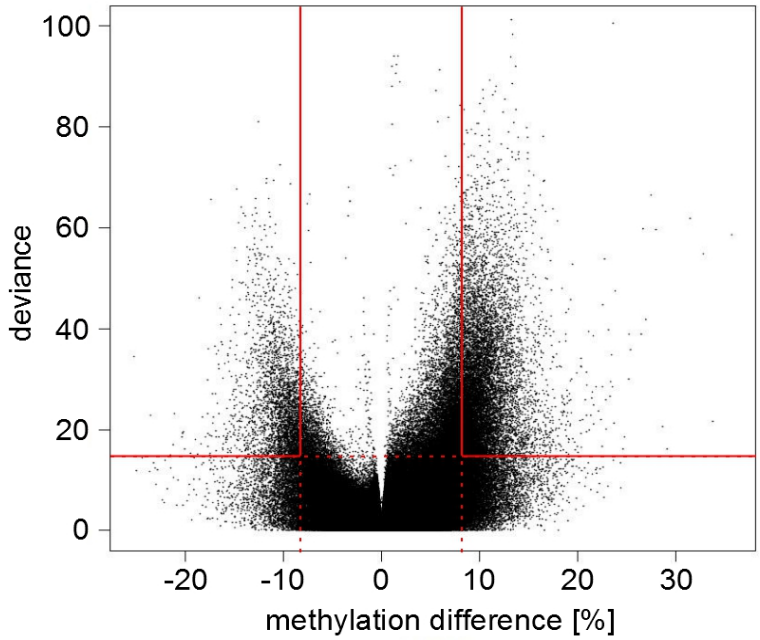

Figure 8: Volcano plot of deviance (y-axis) vs. difference (x-axis) comparing CpG methylation prior to and after SNL procedure. Each point represents a CpG. Points displaying both a deviance > 15 (corresponding to $p \leq 10^{-4}$) and an absolute methylation difference > 8% between the two experimental conditions were defined as "dynamically differentially methylated CpGs" (dDMCs). The thresholds are indicated by red lines. Hypermethylation was more pronounced than hypomethylation.

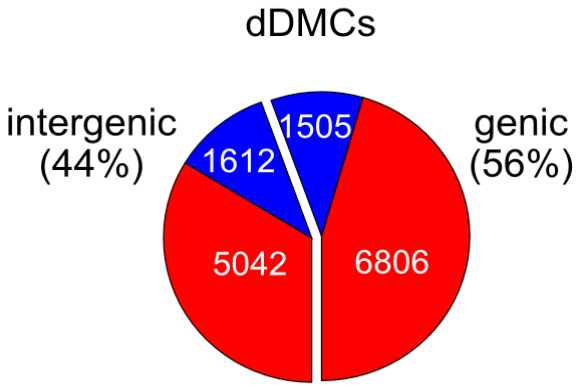

Figure 9: Genome-wide distribution of dDMCs. The majority of the CpG undergoing statistically significant hyper- or hypomethylation in response to nerve injury, dDMCs, were discovered in genic regions or promoters, 56% of dDMCs in the study.

4.3 Analysis of genes and promoters

The injury-related DMCs (dDMCs) were widespread and occurred in genic features in up to 56% of the cases. Figure 10 shows the distribution of these DMCs relative to the total CpGs captured by RRBS in different features (promoter, exon, intron, CGI, CGI shore and intergenic regions). CpGs located in promoters of LCP genes were particularly susceptible to changes. By contrast, HCPs and CpG islands (CGI) remained essentially unaffected by the alterations, which is consistent as CGI are largely located inside HCPs. This finding is in line with previous observations by others [43, 54] and plausible as CGI were more frequently found to be associated with house-keeping genes rather than with tissue-specific genes [51, 52, 57]. Previous observations by others showed that CpG island shores, i.e. regions ≥ 2kb surrounding a CpG island with a comparatively lower CpG density, are particularly susceptible to methylation changes [58, 60]. While we also detected more dDMCs in CpG island shores as compared to the CpG island itself, only a moderate enrichment of dDMCs in this feature was observed.

4.4 Nervous system signaling genes are differentially methylated

Next, we investigated whether any functional role could be attributed to the observed epigenetic alterations. 2,478 genes or promoters containing dDMCs were found. An integrated analysis of these features was performed through pathway analysis (see methods). The core analysis was carried out without prior filtering for molecules related to the nervous system in order to obtain an unbiased interpretation. Of all molecular functions, axon guidance was the top enriched pathway with 98 genes (21% of pathway members) found to be differentially methylated, a highly significant result ($p<10^{-11}$) depicted in Figure 11. For 97 of these genes, CpG methylation was available in the gene body. 93 of these genes harbored methylation changes within the gene body. Of 75 genes, for which promoter CpG information was available, 15 genes harbored changes in the promoter (9 of these harboring changes in the promoter and the gene body and 6 genes harboring changes only in the promoter). These results suggest that CpGs located in the gene body were more susceptible to methylation changes than those located in the promoter region. The list of the 98 axonal guidance genes harboring dDMCs is provided in Table 2.

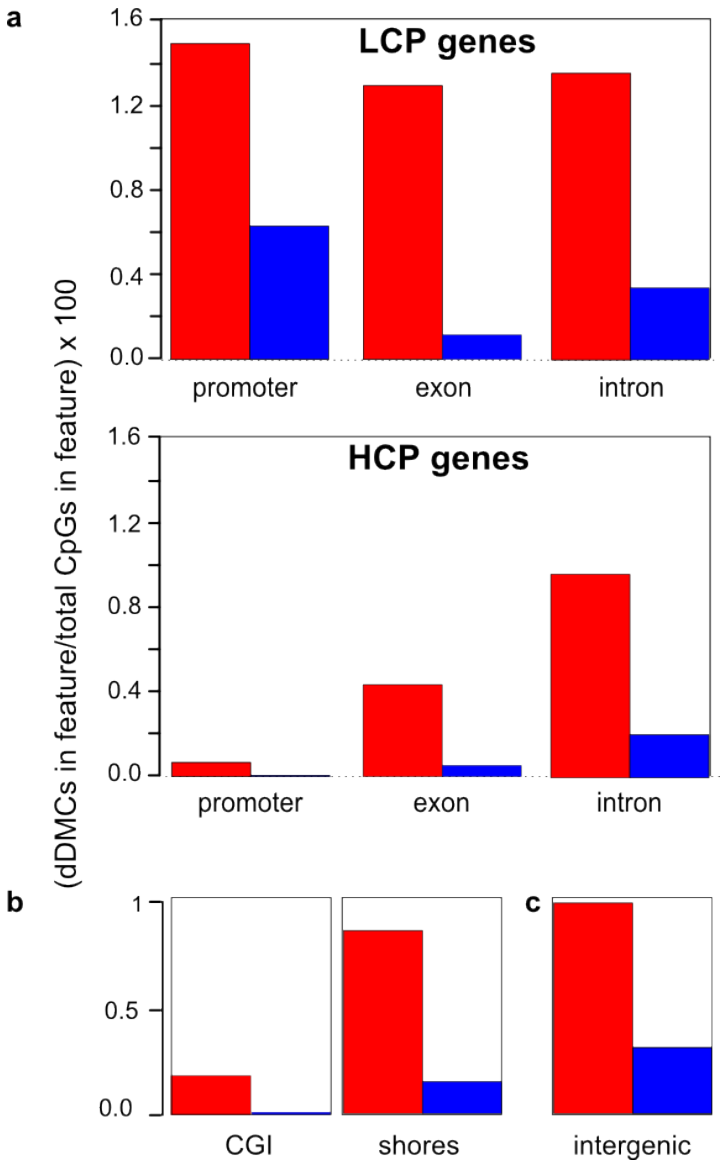

Figure 10: Gene types and other genomic features undergoing hyper- and hypomethylation. The fraction of CpG with significantly altered methylation was calculated across different features for the entire dataset. **a.** Low CpG content promoter (LCP) genes and high CpG content promoter (HCP) genes differed. LCP genes were altered in promoter, exons and introns. HCP genes harbored a comparable fraction of altered methylation sites only in exons and introns, while HCP gene promoters were unaffected. **b.** CpG islands (CGI) remained largely stable, whereas the regions surrounding them—CpG island shores—underwent alterations. **c.** As other independent feature, intergenic regions were enriched in dDMCs.

For a,b,c: Hypermethylation (red) accounted for a greater fraction of changes than hypomethylation (blue) in all regions.

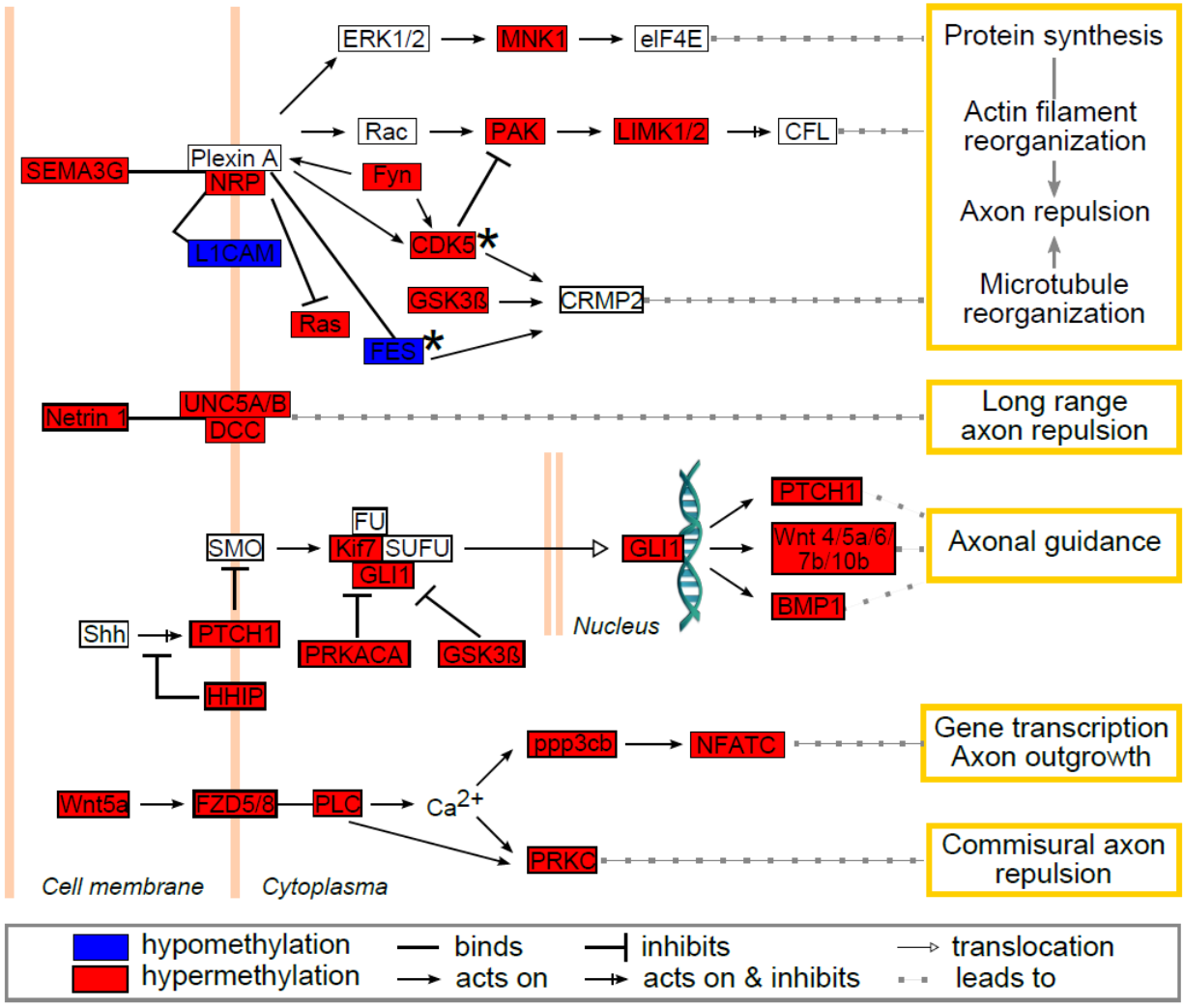

Figure 11: Axon guidance pathway genes differentially methylated after SNL. The most significantly enriched molecular mechanism in an unbiased global analysis of genes undergoing differential methylation after SNL was the axon guidance pathway ($p<10^{-11}$). Depicted are 35 differentially methylated genes with dense connectivity. Variable methylation predominantly occurred in the gene body. Only FES and CDK5 showed methylation alterations in their promoter (black stars). 98 of 468 axon guidance pathway genes were differentially methylated (complete list provided as Table 2).

ENSEMBL ID	Gene name	Direction	ENSEMBL ID	Gene name	Direction
ENSRNOG00000013687	ABLIM1	hyper	ENSRNOG00000020482	NFATC4 *	hyper
ENSRNOG00000019365	ABLIM3	hypo	ENSRNOG00000010744	NRP1 *	hyper
ENSRNOG00000007503	ADAM17	hyper	ENSRNOG00000031232	NRP2	hyper
ENSRNOG00000012424	ADAM23	hyper	ENSRNOG00000003947	NTN1	hyper
ENSRNOG00000001606	ADAMTS5	hyper	ENSRNOG00000018839	NTRK2	hyper
ENSRNOG00000023257	ADAMTS9	hyper	ENSRNOG00000001747	PAK2	hyper
ENSRNOG00000028629	AKT1 *	hyper	ENSRNOG00000029938	PIK3C2B	hyper
ENSRNOG00000008924	ARHGEF12	hyper	ENSRNOG00000034228	PIK3C2G	hyper
ENSRNOG00000004566	ARHGEF15	hyper	ENSRNOG00000016846	PIK3CD *	hyper
ENSRNOG00000004049	BAIAP2	hyper	ENSRNOG00000032238	PLCD1	hyper
ENSRNOG00000010890	BMP1	hyper	ENSRNOG00000014276	PLCE1	hyper
ENSRNOG00000017505	C9orf3	hyper	ENSRNOG00000013676	PLCG2	hyper
ENSRNOG00000008017	CDK5 *	hyper	ENSRNOG00000007970	PLXNC1	hyper
ENSRNOG00000033099	DCC	hyper	ENSRNOG00000007757	PPP3CB	hyper
ENSRNOG00000018683	DOCK1	hyper	ENSRNOG00000005257	PRKACA	hyper
ENSRNOG00000008996	DPYSL5	hyper	ENSRNOG00000009085	PRKAG2	hyper
ENSRNOG00000016203	EFNA2	hyper	ENSRNOG00000028733	PRKAR1B	hyper
ENSRNOG00000034177	EFNA5	hyper	ENSRNOG00000003491	PRKCA	hyper
ENSRNOG00000014648	EFNB2	hypo	ENSRNOG00000012061	PRKCB	hyper
ENSRNOG00000037340	EPHA10	hypo	ENSRNOG00000015603	PRKCE	hyper
ENSRNOG00000007865	EPHB1	hyper	ENSRNOG00000019057	PRKCQ	hyper
ENSRNOG00000012531	EPHB2	hyper	ENSRNOG00000015480	PRKCZ	hyper
ENSRNOG00000031801	EPHB3	hyper	ENSRNOG00000019354	PTCH1	hyper
ENSRNOG00000011683	FES *	hypo	ENSRNOG00000030124	PTPN11	hyper
ENSRNOG00000000596	FYN	hyper	ENSRNOG00000001149	PXN	hyper
ENSRNOG00000014678	FZD5	hyper	ENSRNOG00000024501	RGS3	hyper
ENSRNOG00000038571	FZD8	hyper	ENSRNOG00000012258	RRAS2	hyper
ENSRNOG00000014883	GIT1 *	hyper	ENSRNOG00000016512	SEMA3B *	hyper
ENSRNOG00000025120	GLI1	hyper	ENSRNOG00000018952	SEMA3G	hyper
ENSRNOG00000004766	GLIS2	hyper	ENSRNOG00000019737	SEMA4A *	hypo
ENSRNOG00000005210	GNAI1	hyper	ENSRNOG00000006784	SEMA4F	hyper
ENSRNOG00000016592	GNAI2	hyper	ENSRNOG00000004033	SEMA6A	hyper
ENSRNOG00000019482	GNAO1	hyper	ENSRNOG00000021101	SEMA6C	hyper
ENSRNOG00000019570	GNG3 *	hyper	ENSRNOG00000007687	SEMA7A	hyper
ENSRNOG00000039350	GNG13 *	hyper	ENSRNOG00000029931	SHANK2	hyper
ENSRNOG00000002833	GSK3B	hyper	ENSRNOG00000026065	SLIT1	hyper
ENSRNOG00000018268	HHIP	hyper	ENSRNOG00000007377	SLIT3	hyper
ENSRNOG00000001706	KALRN	hyper	ENSRNOG00000006509	SRGAP3	hyper
ENSRNOG00000026857	KIF7	hyper	ENSRNOG00000031707	TUBA3A *	hyper
ENSRNOG00000011572	KLC1	hyper	ENSRNOG00000003597	TUBA4A *	hyper
ENSRNOG00000037274	L1CAM	hypo	ENSRNOG00000018371	TUBB6	hyper
ENSRNOG00000001470	LIMK1	hyper	ENSRNOG00000025920	UNC5A	hyper
ENSRNOG00000019000	LIMK2	hyper	ENSRNOG00000000567	UNC5B	hyper
ENSRNOG00000017193	LINGO1	hyper	ENSRNOG00000018406	WIPF1 *	hyper
ENSRNOG00000010381	MKNK1	hyper	ENSRNOG00000013166	WNT4	hyper
ENSRNOG00000017539	MMP9	hyper	ENSRNOG00000017409	WNT6	hyper
ENSRNOG00000020246	MYL9 *	hyper	ENSRNOG00000014393	WNT10B	hyper
ENSRNOG00000017146	NFATC1	hypo	ENSRNOG00000015618	WNT5A	hyper
ENSRNOG00000012175	NFATC2	hypo	ENSRNOG00000015750	WNT7B	hyper

Table 2: Axonal guidance genes harboring dDMCs in their gene body or promoter. Genes with differentially methylated promoters are marked by stars (*).

As suggested by the pathway analysis, genes that underwent methylome remodeling highlighted neurobiologically relevant molecular mechanisms known to be involved in the response of the PNS to injury or development of neuropathic pain. This plasticity further extends to genes that are not listed as members of the axonal guidance pathway, yet play recognized roles in the nervous system. Three such examples are provided in Figure 12, namely HCN2, FZD5 and SHANK3. HCN2 is an ion channel which is highly expressed in small DRG neurons. Mice in which HCN2 was knocked-out in these nociceptive primary sensory neurons did not experience neuropathic pain after nerve lesion, emphasizing the role of HCN2 in pain modulation [88]. The G-protein-coupled Wnt receptor Frizzled-5 (FZD5) belongs to the Wnt-signaling-pathway and has been shown to play a role in the establishment of neuronal polarization in the CNS of mice [89]. SHANK3 is a scaffold protein in the postsynaptic density which has a known role in synaptogenesis [90] and is necessary for an accurate excitatory synaptic transmission [91]. In all three examples, changes in methylation were noted in clusters of juxtaposed CpGs and occurred in the gene body.

It is worth noting that many other genes with undefined direct implication in neuroplasticity were also affected by spinal nerve ligation.

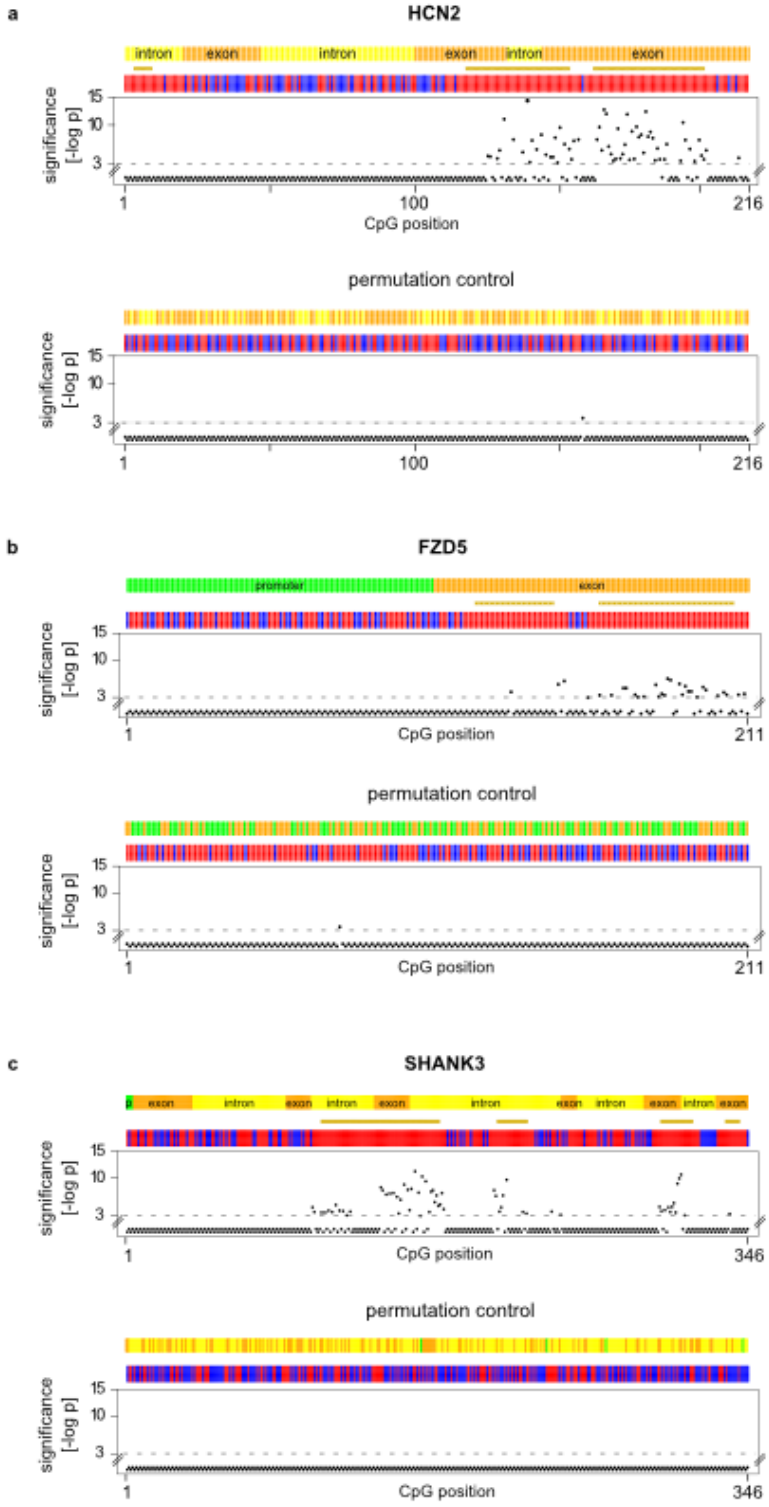

Figure 12: Nucleotide-resolution analysis of three genes with known roles in the nervous system. The methylation profiles of HCN2, FZD5 and SHANK3 are shown in the top panels of a,b,c, respectively. CpG position: The position of captured CpG site

within a gene is indicated (x-axis). Significance at nucleotide resolution: The negative log-p value of the significance level computed by a likelihood ratio test using a generalized linear model (GLM) is shown (y-axis). Higher values indicate stronger significance. Differences with a $p>10^{-3}$ were considered non-significant (CpG positions shown below the dotted line). For all 3 genes differences at individual CpG sites were highly significant ranging from $p<10^{-3}$ to $p<10^{-14}$. Direction of change: The bars in the colored band above the scatterplot indicate for each CpG whether the mean methylation level was higher (red) or lower (blue) in the SNL group compared with controls. The direction of change is shown regardless of significance at the level of a specific CpG. Significance at the region level: Regions that are significantly changed ($p<10^{-3}$) according to a sign test of the direction of juxtaposed CpGs (brown stars).

Top panel of a,b,c: Changes in methylation occurred in clusters of juxtaposed CpGs.

Bottom panel of a,b,c: Random permutation of group assignment and CpG positions confirmed that both statistical testing procedures were robust as indicated by low false positive rates of 0.004, 0.005 and 0 for single CpG testing of HCN2, FZD5 and SHANK3, respectively (1/216, 1/211 and 0/346 CpG above significance threshold) and of 0 (no false-positive) for regions.

4.5 Methylome-transcriptome analysis

To explore a possible relationship of dDMC with the dynamic regulation of gene expression, RNA-seq was performed in DRG harvested 24h after SNL or a control procedure (same as for RRBS above). We profiled 22,908 genes out of which 10,315 genes fulfilled both the quality and quantity criteria and were included in the analysis (see methods). The distribution is provided in Figure 13. As expected, a considerable proportion of genes were induced or suppressed in response to SNL, 2,938 (28.5%) in the present study.

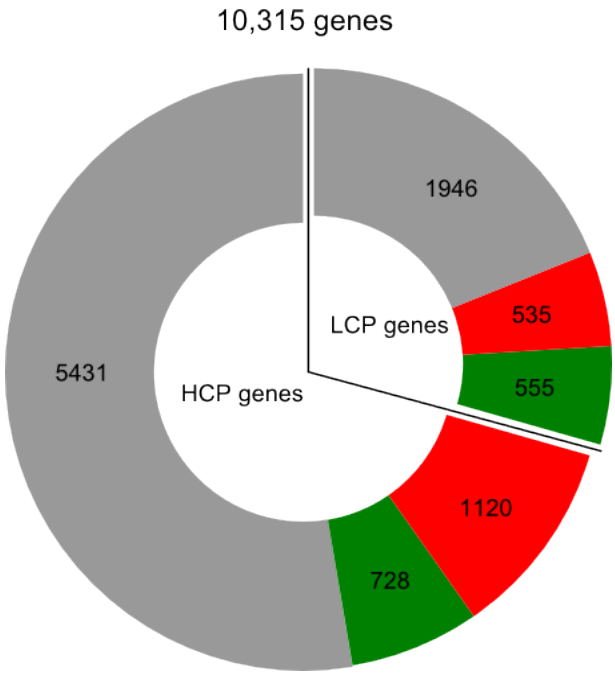

Figure 13: Gene expression profiles of the 10,315 genes included for methylome-transcriptome analysis. Overall, the majority of genes, i.e. 71.5% (7377) remained unaffected by spinal nerve ligation (grey) at a 24h timepoint. LCP genes were more responsive to SNL with 36% of their members getting dysregulated, as compared to 25% for HCP genes (red: upregulation of ≥ 1.5 fold, green: downregulation of ≥ 1.5 fold).

To ascertain that the SNL surgery worked properly, we first looked at genes known to be differentially expressed following SNL procedure. A few reference examples are provided in Table 3, validating the results obtained by others.

Gene name	Fold change (log_2)	Full name	Reference
ATF3	6.2	Activating transcription factor 3	[92]
A2m	5.8	Alpha-2-Macroglobulin	[93]
NGF	3.4	Nerve growth factor	[94]
SOCS3	5.0	Suppressor of cytokine signaling 3	[95]
SOX11	4.2	SRY (sex determining region Y)-box 11	[96]
STAT3	1.0	Signal transducer and activator of transcription 3	[95]

Table 3: Expression changes of genes known to be dysregulated following nerve injury

When next looking at the subset of dysregulated genes mentioned in Table 3, no significant alteration of their methylation profiles was detected. Only limited information was available for A2m and NGF (8 and 16 CpGs captured by RRBS respectively, all located in introns), making it difficult to draw meaningful conclusions between methylation changes and gene expression changes, as no information of the behavior of CpGs located in the promoter regions and exons was obtained. However, for each of the other examples, data of the methylation status of 60 to 234 CpGs distributed across promoters, exons and introns was assessed, and no significant methylation changes observed. Similarly, when focusing on the example genes HCN2, FZD5 and SHANK3 whose methylation profiles were altered after SNL (Figure 12), no significant dysregulation of their expression was observed.

As has been proposed in the past [97], genes where promoter methylation was associated with gene downregulation (29 genes) were found. However, a similar fraction (36 genes) was upregulated when the promoter was hypermethylated. Conclusions that are based on individual genes are therefore not sufficient when attempting to find a systematic association between methylome and transcriptome changes.

In order to examine whether a genome-wide trend relating methylome and transcriptome alterations could be found, an integrated analysis of dDMCs and gene expression changes was performed. Based on prior observations suggesting that (1)

HCP genes and LCP genes were regulated differently [54, 56, 57] and (2) the effects of promoter and gene body methylation diverged [27, 98], we analyzed these scenarios separately. Genes that were dysregulated by nerve damage and harbored dDMCs in their promoter or gene body were identified. Figure 14 illustrates the relationship between gene expression and methylation changes in promoters and gene bodies of HCP- (a and b) and LCP genes (c and d), respectively. The promoter regions of HCP genes were poorly enriched for dDMCs (see Figure 14d). The dDMCs that were associated with dysregulation of the corresponding gene are shown in Figure 14a and represent 33% of dDMCs in this genomic location. A similar number of genes was found to be up- and downregulated when a dDMC was hypermethylated, 21 and 16 genes respectively. We found 152 dysregulated HCP genes that harbored dDMCs in their gene body. The majority of these dDMCs gained methylation after SNL (Figure 14b). This went along with changes of gene expression in both possible directions. Similar results were obtained for dDMCs that lost methylation.

As expected, a lower absolute number of dDMCs associated with gene dysregulation was found in the promoter and gene body of LCP genes (Figure 14c and 14d). LCP genes contain few CpGs, which are therefore less likely to be captured by RRBS as compared to CpGs located in HCP genes. Yet, CpGs captured in LCP were more frequently differentially methylated than those located in HCP (Figure 10a). Differential methylation of LCP was associated with dysregulation of 30% of the affected genes. Hypermethylation was predominant but no directional trend for transcriptome alteration was observed (Figure 14c). When next considering dDMCs located in the gene body of LCP genes, both methylation gain and loss were observed in association with gene up- and downregulation (Figure 14d).

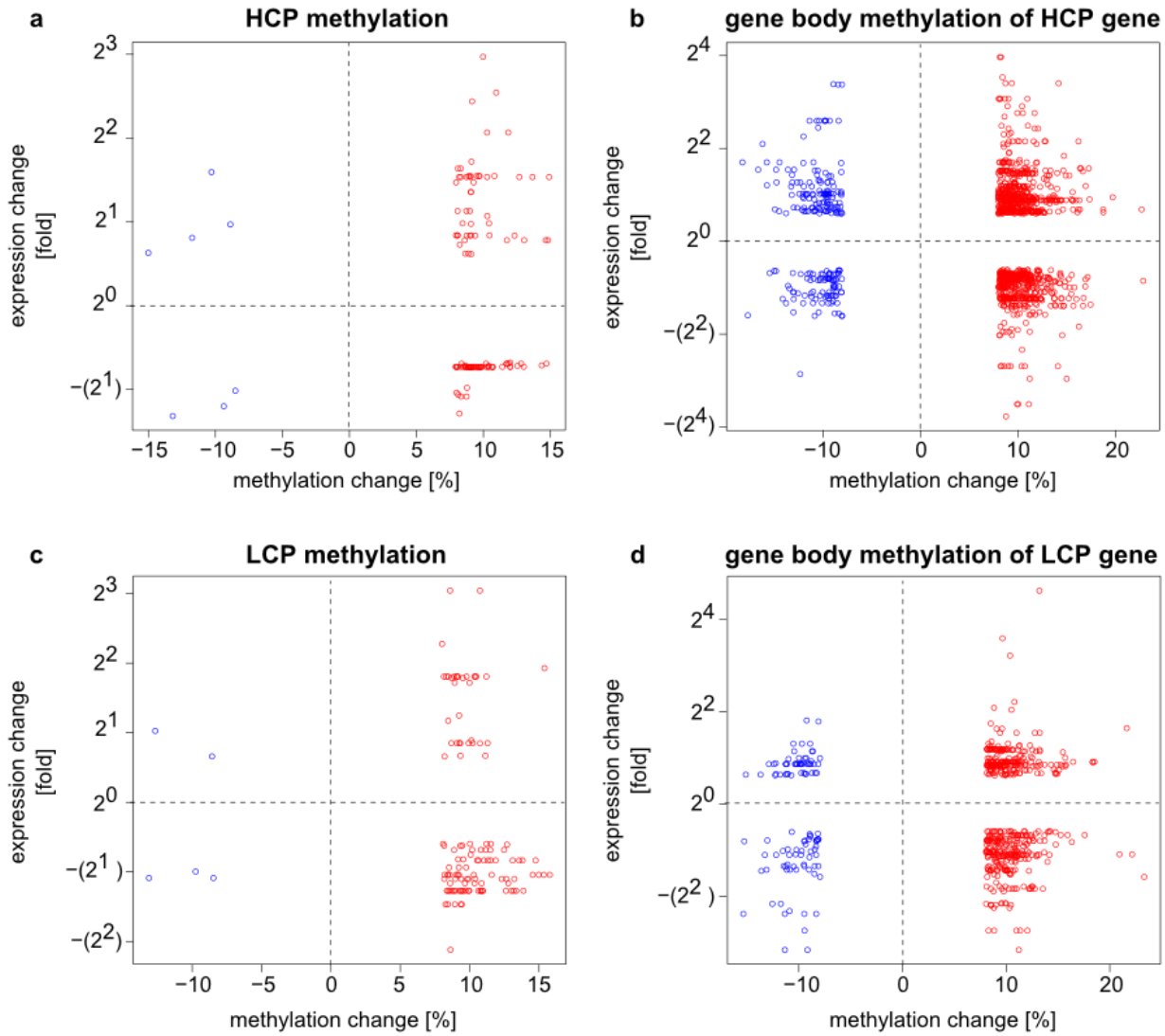

Figure 14: Transcriptome up- and downregulation can co-exist with CpG hyper- or hypomethyation in the promoter and gene body. An integrated transcriptome-methylome analysis supported a negative finding, notably the absence of any tight correlation between transcriptome- and methylome alterations following SNL. Shown is the direction of CpG methylation change and gene expression change following nerve injury. Genes were divided into two groups: high CpG promoter (HCP; panel a and b) and low CpG promoter (LCP) genes (panel c and d). Promoter- (left, panel a and c) and gene body methylation (right, panel b and d) were analyzed separately. The methylation levels of dDMCs (x-axis) were plotted against the expression value of their corresponding gene (y-axis). Each circle represents a differentially methylated CpG (dDMC), thereby allowing multiple pairings of individual dDMCs with the same gene. The analysis was performed with significantly changed CpG sites located in genes that

underwent a significant change in expression. The results shown demonstrate that all possible scenarios exist hyper- and hypomethylation of CpG associated with increase or decrease in RNA levels from the same gene. Red: hypermethylated dDMC, blue: hypomethylated dDMC.

4.6 Plasticity extends to gene deserts

4.6.1 Arrangement of methylation changes in intergenic regions

Methylome alterations in the nervous system have to date been interpreted in the context of genes. Yet the present study—thanks to its unbiased genome-wide ascertainment of methylation levels—found 44% of dDMC in gene deserts, dDMC in non-annotated regions of the genome (see Figure 9). Analyzing these intergenic regions, a CpG was equally likely to be a dDMC regardless of its distance to the most nearby gene, supporting the classification of this dDMC subset as "desert" (Figure 15).

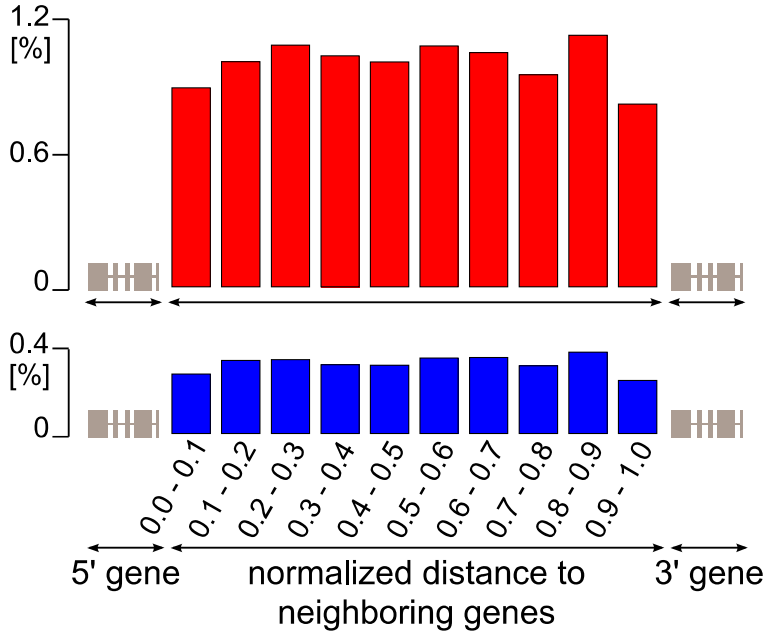

Figure 15: dDMCs in gene deserts. Nearly half of the CpGs undergoing statistically significant hyper- or hypomethylation in response to nerve injury, dDMCs, were discovered in intergenic regions, 44% in the study. The distribution was even across the intergenic span as seen from the combined analysis of the location of 5042 hyper- and 1612 hypomethylated sites (right). The likelihood of a CpG to be differentially methylated after SNL was independent of its distance from the closest gene. thereby validating the classification of all these sites as "desert dDMCs".

We next investigated whether the intergenic alterations were randomly distributed across the gene deserts or followed a specific pattern. Therefore, an in silico window of 100bp was slid over the gene deserts and extended as soon as a dDMC was reached. This procedure revealed that dDMCs occurred in clusters and that inside a cluster, neighboring dDMCs varied in the same direction. This result is shown in Figure 16 and suggests a well organized structure of dDMC events despite the lack of a gene structure.

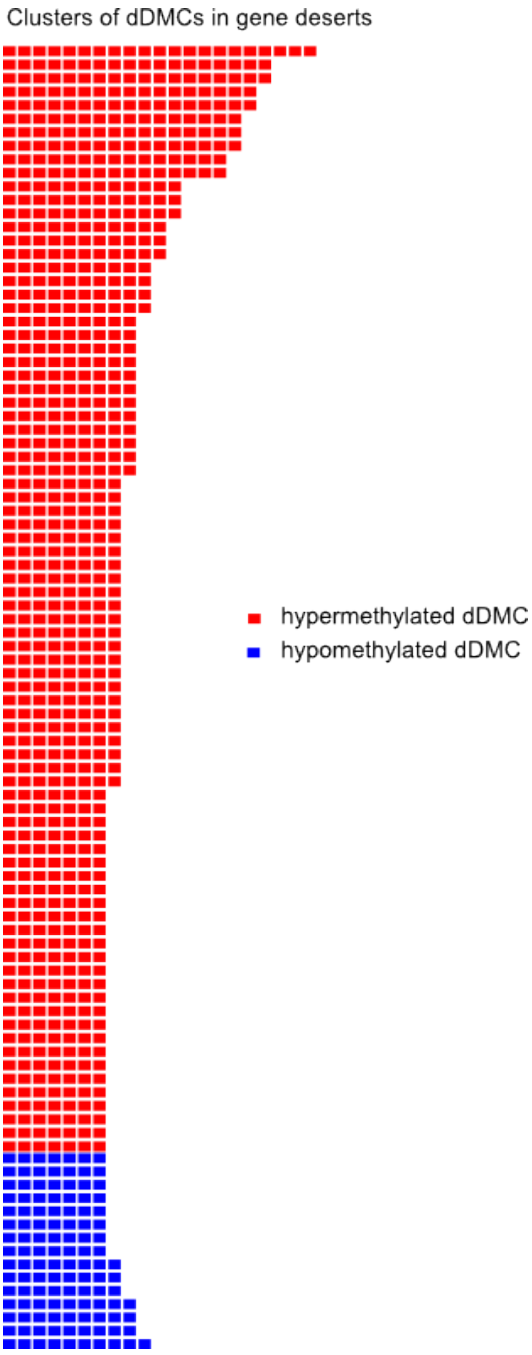

Figure 16: Uniformity of desert dDMC clusters. Neighboring dDMCs in gene deserts underwent unidirectional methylation change forming clusters. To minimize chance events only clusters consisting of ≥ 5 dDMC members were examined, corresponding to > 80% of the data. Non-randomness was significant with $p<0.05$ to $p<2x10^{-6}$ for sizes ranging from 7 to 21. Red and blue represent hyper- and hypomethylation, respectively.

4.6.2 Positional prediction of intergenic dDMCs by an organism-wide methylome model

To test whether the intergenic dDMCs between L5 control and L5 SNL (1st experimental dataset) were randomly or systematically spread across gene deserts, we sought to determine whether functional methylome plasticity in desert regions occurring in response to PNS damage—dDMCs—can be predicted from a genome-biology guided, organism-wide analysis of the methylome. Therefore a comparative analysis of the 1st experimental dataset with a 2nd, independent experimental dataset consisting of muscle, spleen, liver and L4 DRG was performed. Only CpGs with a read coverage ≥10 that were common to all samples of both sets, resulting in 368,147 intergenic CpGs were considered for all calculations below.

First, using only the 2nd experimental dataset we found that a substantial number of intergenic CpGs, 40%, was differentially methylated in at least one of the four tissues (tissue-specific differentially methylated, tDMCs), while the remaining, 60%, were identical in all organs (tissue invariant methylated CpG, tIMC). Based on the intergenic CpGs, the DRG methylome could readily be distinguished from other tissues (Figure 17). An example region where the methylation pattern of the DRG differs from the three other tissues is provided in Figure 18, as well as a tissue-invariant region.

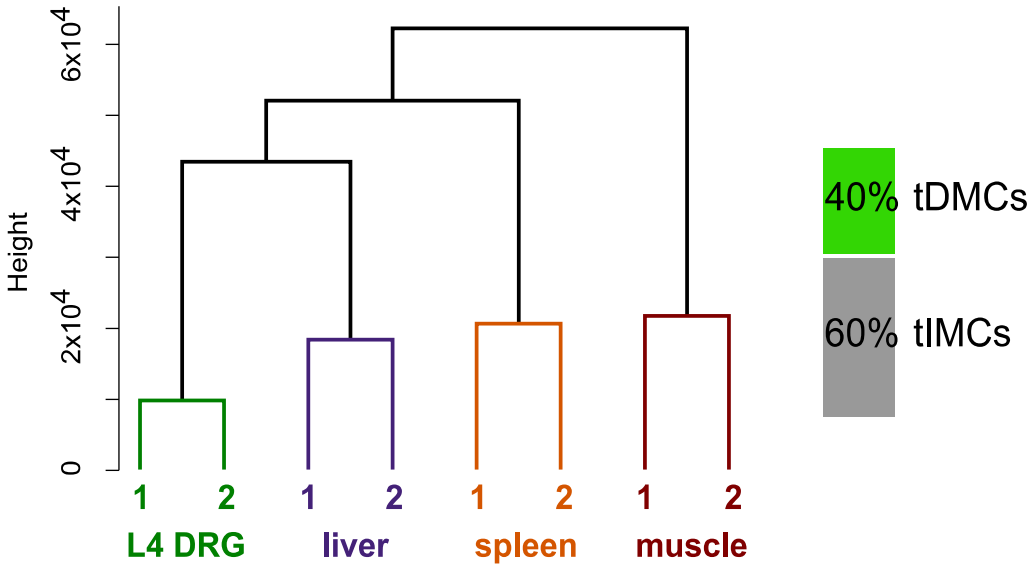

Figure 17: Hierarchical clustering analysis confirmed organ-specific methylation of gene deserts (right). 2 replicates were available for each tissue.

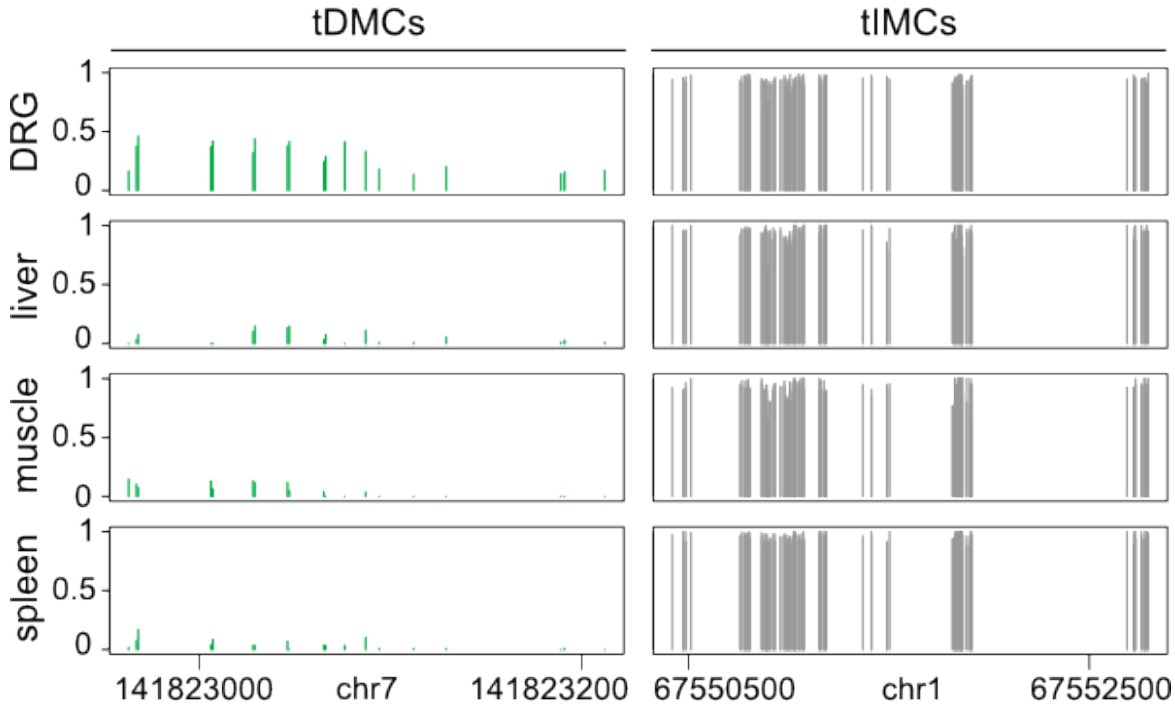

Figure 18: Methylation profiles of a DRG-specific gene desert and an invariant intergenic region. Cytosine methylation sites of the 2nd experimental dataset were dichotomized into tissue-specific differentially methylated CpG (tDMCs) and tissue-invariant methylated CpG (tIMCs), demarcating regions that have distinct methylation patterns, tDMCs, and others that were equally methylated in all organs, tIMC. Rat control DRG (new replicates), spleen, muscle, and liver were compared. Sample regions with tDMCs and tIMCs are shown. The absolute methylation level is represented on the y-axis.

Second, we tested the hypothesis that the methylome response to nerve injury, dDMCs, would occur only in one of the two types of regions defined by tissue comparison, i.e., either in the tDMC or the tIMC region. Notably, the location of the vast majority, > 97% of the 5,502 CpGs remodeled after SNL (dDMCs), overlapped with CpGs that were identified as plastic between tissues in the 2nd experimental dataset, the tDMCs (Figure 19). The odds ratio for the enrichment was OR=58 (5360 x 220354)/(142291 x 142), which is highly significant ($p<10^{-15}$).

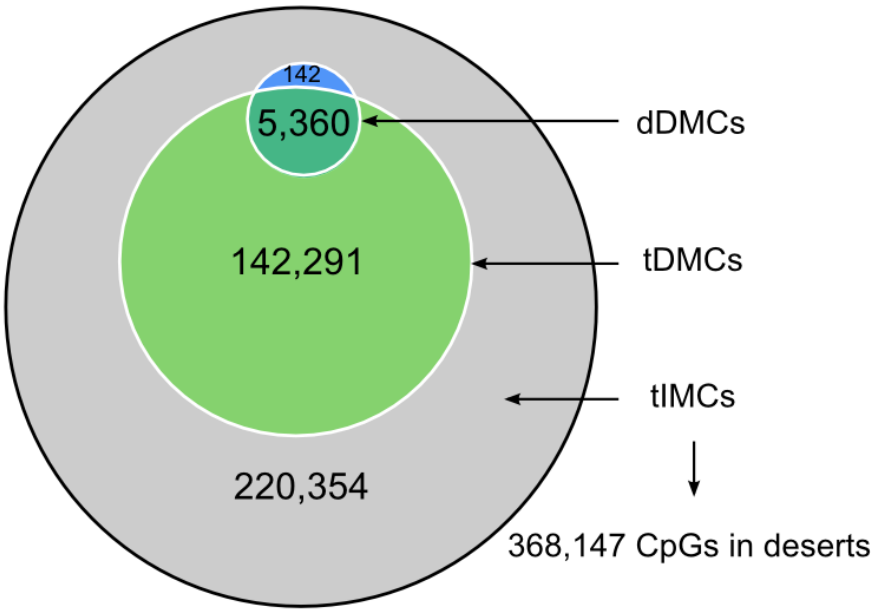

Figure 19: Desert remodeling after SNL (dDMCs) affects the same CpG sites that are differentially-methylated between tissues (tDMCs). CpG undergoing methylation changes in response to SNL, dDMCs, were a subset of tDMCs. The enrichment of dDMCs in the tDMC vs. tIMC subsets of CpG sites was highly significant ($p<10^{-15}$). Gene desert methylation can be divided according to a dual model: The majority of CpG methyl-marks remain stable organism-wide regardless of tissue type or pathology; a substantial minority of CpG methyl-marks, tDMCs, are dynamic and encompass all sites capable of responding to changes in the environmental such as at the CpG sites identified in the present study as dDMCs through their response to nerve injury.

The preferential location of dDMCs suggests a dichotomy of the intergenic methylome in an invariant part—which remains stable across different tissues and conditions (demarcated by tIMCs)—and a plastic part that is more susceptible to alterations and encompasses CpG sites capable of responding to environmental changes such as nerve injury (dDMCs).

4.6.3 Plastic and invariant deserts differ in their binding site motif

The new distinction raised the possibility that the two types of gene deserts might differ in regard to the genomic sequence patterns. The possibility was tested by performing an analysis for known DNA binding site sequence motifs. To this purpose, gene deserts were split into regions that were hyper-, hypomethylated or invariant in SNL as

compared to the control. This resulted in 1006 hyper-, 377 hypomethylated and 81,600 invariant intergenic regions. HOMER software (hypergeometric optimization of motif enrichment) was implemented on these regions for motif enrichment analysis. The invariant regions were set as background and the hyper- or hypomethylated regions as foreground to look for motifs that were overrepresented in one or the other group. Plastic intergenic regions were found to be markedly different from invariant regions. Interestingly, while the analysis took an unbiased approach considering the entire universe of eukaryotic DNA binding proteins, the top enriched DNA motifs matched transcription factors with important roles in PNS development, regeneration, and sensory dysfunction. Hypomethylated plastic deserts were most markedly enriched for ETS binding ($p<10^{-38}$), which was noteworthy because ETS binding controls the transcription of axotomy-responsive genes in the DRG [99]. Binding sites of the RUNX gene family of transcription factors was the other top enriched motif ($p<10^{-31}$) with Runx1 sites driving the result. Runx1 determines the nociceptive sensory neuron phenotype and is required for thermal and neuropathic pain [100]. Other Runx proteins have been reported to control the axonal projection of proprioceptive DRG neurons [101]. Hypermethylated plastic deserts were enriched for SOX gene family- ($p<10^{-51}$) and neurofibromin 1 (NF1) binding sites ($p<10^{-22}$). SOX genes are involved in neuronal development [102] and axon regeneration [103] and NF1 has long been recognized for its critical role in the PNS.

5 Discussion

The present study examined DNA methylation in the PNS in a rodent model of neuropathic pain. The main hypothesis that spinal nerve injury can modify the methylome of the dorsal root ganglion was verified. This work provides results on a genome-wide scale with nucleotide resolution analyzing methylome alterations in both genic and non-genic regions. The methylome remodeling of genes known as regulators of the PNS response to injury and chronic pain matches predictions made by some authors in recent years [4]. Additionally, the early onset of these changes suggests that DNA methylation is a highly dynamic process, playing a previously underestimated role in the response of the PNS to nerve injury.

The only previous publication in the field of neurobiology reporting genome-wide dynamic methylome alterations is by Guo et al., studying CpGs in genic regions using mixed tissue from the mouse hippocampus after electrostimulation [43]. The present study corroborated the observation by Guo et al. that methylome alteration in the adult nervous system can occur rapidly and that CpG islands are epigenetically stable. Interestingly, we found like Guo et al. that hypermethylation was more common than hypomethylation.

Like all organs, the DRG comprises a mixture of cell populations, presumably characterized by different methylation profiles. Analysis of such mixed tissues has been routinely performed previously, but results need to be interpreted with appropriate caution. Following nerve injury, the neural response is accompanied by the activation of satellite cells and the infiltration of macrophages and T-lymphocytes through blood vessels and meninges [12, 94, 104]. These mechanisms potentially contribute to the observed methylome alterations. Little is known about the exact amount of immune cells in the DRG at a 24h-timepoint after nerve injury. Hu & Mclachlan found that one week after spinal nerve transection the density of macrophages in the corresponding ipsilateral DRG was about four times greater than in the controls. This elevation persisted at a later timepoint of 11 weeks [104]. T-lymphocytes were dramatically elevated at a one week timepoint (30-fold) and regressed to a 20-fold level at 11 weeks as compared to controls. Another study reported that the number of macrophages in the DRG started to increase 2-4 days after sciatic nerve transection and remained elevated

for four weeks [105]. In the present study, the glial fibrillary acidic protein (GFAP), an astroglial marker which is also expressed by satellite cells [104] was 50-fold upregulated, emphasizing that glial activation took place within 24h of nerve injury. In the present study, methylome remodeling affected genes that were previously shown to be neuron-specific, such as OZD2 and PCSK2 [106]. Similarly HCN2, whose methylation changes are depicted in Figure 12, is strongly expressed in primary sensory neurons [88]. The binding motif analysis of differentially methylated intergenic regions yielded an enrichment for transcription factors that play important roles in the PNS and further supports the involvement of neuronal cells in the methylome response to injury. These findings—along with the highly significant enrichment of axonal guidance genes—suggest that methylome remodeling occurred in neurons as well as possibly in glial cells.

To examine how the plasticity of the PNS methylation landscape evolves after the initial tissue inflammation has ceased, further studies at later time-points will be required. Yet, the problem of tissue-mixture will persist until technical advances will allow a convenient separation, extraction and qualitative amplification of single cells or distinct cell groups. Approaches such as the laser capture microdissection [107] enable the harvesting of cells of interest from a tissue section under microscopic visualization by cutting and capturing the cells using laser energy; yet the procedure remains laborious and costly and has therefore not established itself as standard in the field. Single-cell sequencing is the most recent technical challenge [108]. While this approach would yield insights into the functionality of a single cell, the technique is still limited, as the very small starting amount of DNA is compounded by the even more negative effects of contamination, erroneous genome amplification and uneven coverage, thereby diminishing the sequence quality [109]. Once these problems are overcome, the combination of single-cell amplification and bisulfite sequencing will shed light on the methylome of individual sensory neurons—or rather on the new subgroups of neurons that will be identified.

Using RRBS, ~3% of all genomic CpGs in the rat were captured. Comprehensiveness of analysis, resolution of exact genome position, and experimental resource requirements are recognized competing features in the design of unbiased epigenomics studies. While RRBS is most efficient for CpG-rich regions, its “reduced representation”

has been found repeatedly to provide highly informative genome-wide extrapolation. A comparative analysis of whole genome bisulfite sequencing (WGBS) and RRBS demonstrated that for all the genomic regions covered by both techniques, the coverage depth obtained by RRBS was approximately five times higher as compared to WGBS [110]. This result is noteworthy when interpreting the accuracy of methylation levels. Furthermore, while WGBS benefits from higher resolution, its relative inefficiency was demonstrated by a recent study showing that over 70% of the reads captured by WGBS either did not contain any CpG or suffered from low coverage depth [111]. RRBS therefore enables highly reproducible, quantitative comparisons of methylation levels at single-base resolution and reasonable sequencing cost, making it the technology of choice for CpG methylation analysis.

The bisulfite sequencing methodology underlying RRBS cannot distinguish methyl-cytosine (mC), the principal modification of CpG sites from hydroxy-methyl cytosine (hmC), a rare variant found at up to 2% of modified CpG sites in certain tissues. The first step of gaining a cytosine modification *in vivo* is addition of the methyl mark, C→mC. Hydroxymethylation can only occur as a subsequent step, mC→hmC. Therefore, any new CpG modification that was detected in the present study by RRBS (following SNL) consisted of an obligatory modification C→mC. While some of the newly formed mC might have subsequently been further changed to hmC, the conclusion that gain of mC occurred after SNL is not affected. The opposite case, CpG demethylation, also needs to be considered. In this case, RRBS determined the loss of a CpG modification, which could have occurred at a site that was a mC (most likely) or a hmC (possibly at few sites) at baseline before SNL. Therefore, while RRBS could not resolve whether the DRG methylome consists only of mC marks or includes some hmC modifications, the presented data can be interpreted without ambiguity in regard to the dynamic methylome changes observed after SNL.

The results of the integrated analysis of dDMCs and RNA alterations suggested that anti-correlation (methylation up—transcription down) fell short as a model at least when attempting to explain the dataset in its entirety. This conclusion is consistent with an increasing number of reports of integrated methylome-transcriptome analyses based on high quality datasets proposing that this relationship cannot be represented by a simple model [43, 54, 98, 112, 113]. In the study from Guo et al. 1,819 CpGs that were

differentially methylated in the mouse hippocampus after electrostimulation mapped to 1,518 genes. A modest anticorrelation between promoter methylation and gene expression (r=-0.3) was found, while a lack of correlation was noticed when examining DMCs located in the gene body or around the transcriptional end site. The authors concluded that *de novo* methylation or demethylation may function in ways other than through directly regulating transcription levels. Using the Infinium 27K methylation array, Zouridis et al. compared the methylation profiles of 240 gastric cancers and 94 normal gastric tissues at 27,578 CpG sites and found 41% of these to be differentially methylated (DMCs) [113]. A subset of samples was used to compare 6745 DMCs associated with 4903 genes. In only 25% a correlation between methylation and gene expression could be found, whereby in most of the cases methylation and expression where anticorrelated. The same methylation array was used by Lam et al. to assess DNA methylation in the promoter regions of ~14,500 genes in peripheral blood mononuclear cells of a human community cohort [112]. Different demographic factors as well as early-life socioeconomic status were found to be associated with variable DNA methylation. Across individuals the authors found that the vast majority of variable CpG methylation did not correlate with gene expression. For those CpGs where a correlation with transcription was found, both scenarios of “methylation up - expression down” and “methylation down - expression up” were represented, indicating that alteration in DNA methylation does not necessarily relate to alteration in gene expression. The report by Kulis et al. demonstrated that the 2 molecular subtypes of chronic lymphocytic leukemia (CLL) could be separated based on their methylation patterns [98]. 3,265 DMCs were detected using an Infinium 450k methylation array. When analyzing the relationship between methylation and gene expression, a significant correlation was detected in 4% of all CpGs. For these CpGs, correlations with gene expression were found both between DMCs located in the promoter region and the gene body. Ng et al. explored the methylome of cell lines derived from mouse striatal neurons expressing either the normal huntingtin gene or the mutated form that is responsible for the Huntington disease [54]. Genome-wide methylation was assessed at 97,006 CpG sites using RRBS and revealed a partial loss of methylation in the mutated gene. While the authors found an anticorrelation between methylation in CpG-rich promoter region and transcription, increased or decreased methylation in CpG-poor promoters could result either in

enhanced or diminished expression.

The findings by Ng et al. prompted us to examine promoters of HCP and LCP genes and their respective gene bodies separately. Yet, no correlation with gene expression changes was found (see Figure 14). Overall, the results of the present study are in line with the above mentioned reports and suggest a poor direct relationship between variation in DNA methylation and variation in gene expression.

Issues that need to be resolved in the field in order to better characterize the methylome-transcriptome relationship are plentiful. They include limitations resulting from using tissues rather than single cells; the role of other epigenetic modifications like histone methylation and acetylation; the role of other DNA modifications such as hydroxymethylation that remains difficult to assess with precision at nucleotide resolution; and a recurrent narrative bias in the literature to report an association of methylation gain with gene repression regardless of the biological context.

The present study also pointed to a role of non-genic regions, which was consistent with published reports showing that CpG methylation changes can affect regulatory elements throughout the genome including sites that are far distant from annotated promoter regions [111, 114]. These regions have not been studied before in neurobiology models of disease. To gain some mechanistic understanding of the changes occurring across gene deserts, a detour into organism-wide genome-biology was taken: performing extensive methylation sequencing of various organs with the goal of understanding better what is happening in the PNS. The classification of intergenic regions into plastic and invariant deserts is based on the new type of methylome data that was obtained. There was highly significant statistical support for the prediction of plastic desert CpGs and it was further supported as functionally important by the highly significant binding site enrichment patterns observed.

These findings suggest that methylation of gene deserts may co-determine the function of genes by modulating the configuration of regulatory regions. Recently, Stadler et al. identified low methylated CpG-poor regions that were enriched for DNA binding factor sites in the mouse [114]. By means of two transcription factors, REST and CTCF, the authors showed that binding within these active regulatory regions results in the demethylation of the site and suggested that this process could in turn facilitate the

binding of additional binding factors that are sensitive to DNA methylation. Similarly, Ng et al. showed that the loss of binding of certain transcription factors was strongly associated with increased DNA methylation [54]. However, whether DNA methylation changes precede the binding of transcription factors or are its consequence needs to be fully understood [115].

In the present study HOMER was used to detect the enriched consensus motifs for transcription factor binding sites in the SNL vs. control animals. However, the motif discovery includes base position variability, making it impossible to identify the exact genomic position of these sequences. To further confirm that the mentioned transcription factors are truly bound to regions of dynamically altered DNA methylation, genome-wide chromatin immunoprecipitation sequencing (ChIP-Seq) is required.

Time-course studies are further required to test whether the observed methylome alterations are long lasting and stable over time or return to the initial state after days or weeks. When is the maximum of change reached? Is this state reversible by drugs? It is imaginable that the methylation alterations observed in the present study get more pronounced after several days, thereby following or even controlling the progression of the pain phenotype, which achieves its maximum at 14 days in the SNL model. These questions remain to be elucidated.

Small molecule inhibitors of DNA methyltransferases have been developed for cancer therapy (such as 5-aza-cytidine or RG108). While such drugs would act genome-wide without discriminating PNS-specific alterations, the present study might provide a rationale for testing their potential to prevent or reduce the pain-related consequences of L5 SNL such as allodynia. RG108 which inhibits methylation would be of a particular interest in this context, as an imbalance favoring methylation gain in the DRG was observed after nerve damage. Future animal experiments using the intrathecal application of RG108 are therefore imaginable.

This present work leveraged a current technology, RRBS, providing precise quantification of methylation levels not only for individual genes but specific CpG sites. The approach demonstrated widespread methylome remodeling in the sensory ganglion in response to nerve damage in the rat, affecting two portions of the genome: First, well annotated genic regions such as those of the axon guidance pathway genes. Second,

plastic deserts, regions that were not previously studied in the context of PNS biology, yet appeared to undergo equally marked epigenomic remodeling. The majority of genes and most of gene deserts were invariant in all experimental conditions. Thereby the present study demonstrated methylome stability as well as genome-wide, targeted methylome remodeling in the PNS.

6 References

1. Costigan M, Belfer I, Griffin RS, Dai F, Barrett LB, Coppola G, Wu T, Kiselycznyk C, Poddar M, Lu Y, Diatchenko L, Smith S, Cobos EJ, Zaykin D, Allchorne A, Gershon E, Livneh J, Shen P-H, Nikolajsen L, Karppinen J, Männikkö M, Kelempisioti A, Goldman D, Maixner W, Geschwind DH, Max MB, Seltzer Z, Woolf CJ: Multiple chronic pain states are associated with a common amino acid-changing allele in KCNS1. *Brain* 2010, 133:2519–27.

2. Hammer P, Banck MS, Amberg R, Wang C, Petznick G, Luo S, Khrebtukova I, Schroth GP, Beyerlein P, Beutler AS: mRNA-seq with agnostic splice site discovery for nervous system transcriptomics tested in chronic pain. *Genome Res* 2010, 20:847–60.

3. Michaelevski I, Segal-Ruder Y, Rozenbaum M, Medzihradszky KF, Shalem O, Coppola G, Horn-Saban S, Ben-Yaakov K, Dagan SY, Rishal I, Geschwind DH, Pilpel Y, Burlingame AL, Fainzilber M: Signaling to transcription networks in the neuronal retrograde injury response. *Sci Signal* 2010, 3:ra53.

4. Denk F, McMahon SB: Chronic pain: emerging evidence for the involvement of epigenetics. *Neuron* 2012, 73:435–44.

5. Toth C, Lander J, Wiebe S: The prevalence and impact of chronic pain with neuropathic pain symptoms in the general population. *Pain Med* 2009, 10:918–29.

6. Smith BH, Torrance N: Epidemiology of neuropathic pain and its impact on quality of life. *Curr Pain Headache Rep* 2012, 16:191–8.

7. Farrar JT, Young JP, LaMoreaux L, Werth JL, Poole RM: Clinical importance of changes in chronic pain intensity measured on an 11-point numerical pain rating scale. *Pain* 2001, 94:149–58.

8. Max M, Schafer S, Culnane M, Dubner R, Gracely R: Association of pain relief with drug side effects in postherpetic neuralgia: a single-dose study of clonidine, codeine, ibuprofen, and placebo. *Clin Pharmacol Ther* 1988, 43:363–71.

9. Weber H, Holme I, Amlie E: The natural course of acute sciatica with nerve root symptoms in a double-blind placebo-controlled trial evaluating the effect of piroxicam. *Spine (Phila Pa 1976)* 1993, 18:1433–8.

10. Attal N, Cruccu G, Baron R, Haanpää M, Hansson P, Jensen TS, Nurmikko T: EFNS guidelines on the pharmacological treatment of neuropathic pain: 2010 revision. *Eur J Neurol* 2010, 17:1113–e88.

11. Dworkin RH, O'Connor AB, Backonja M, Farrar JT, Finnerup NB, Jensen TS, Kalso E a, Loeser JD, Miaskowski C, Nurmikko TJ, Portenoy RK, Rice ASC, Stacey BR, Treede R-D, Turk DC, Wallace MS: Pharmacologic management of neuropathic pain: evidence-based recommendations. *Pain* 2007, 132:237–51.

12. Hanani M: Satellite glial cells in sensory ganglia: from form to function. *Brain Res Brain Res Rev* 2005, 48:457–76.

13. Ji R-R, Kohno T, Moore KA, Woolf CJ: Central sensitization and LTP: do pain and memory share similar mechanisms? *Trends Neurosci* 2003, 26:696–705.

14. Neumann S, Doubell TP, Leslie T, Woolf CJ: Inflammatory pain hypersensitivity

mediated by phenotypic switch in myelinated primary sensory neurons. *Nature* 1996, 384:360–4.

15. Okamoto M, Baba H, Goldstein P, Higashi H, Shimoji K, Yoshimura M: Functional reorganization of sensory pathways in the rat spinal dorsal horn following peripheral nerve injury. *J Physiol* 2001, 532:241–50.

16. Neumann S, Braz JM, Skinner K, Llewellyn-Smith IJ, Basbaum AI: Innocuous, not noxious, input activates PKCgamma interneurons of the spinal dorsal horn via myelinated afferent fibers. *J Neurosci* 2008, 28:7936–44.

17. Watanabe K, Konno S, Sekiguchi M, Sasaki N, Honda T, Kikuchi S: Increase of 200-kDa neurofilament-immunoreactive afferents in the substantia gelatinosa in allodynic rats induced by compression of the dorsal root ganglion. *Spine (Phila Pa 1976)* 2007, 32:1265–71.

18. Liu C, Michaelis M, Amir R, Devor M, Lu VB, Colmers WF, Smith PA, Amir RON: Spinal Nerve Injury Enhances Subthreshold Membrane Potential Oscillations in DRG Neurons : Relation to Neuropathic Pain Spinal Nerve Injury Enhances Subthreshold Membrane Potential Oscillations in DRG Neurons : Relation to Neuropathic Pain. *J Neurophysiol* 2000, 84:205–215.

19. Wall PD, Devor M: Sensory afferent impulses originate from dorsal root ganglia as well as from the periphery in normal and nerve injured rats. *Pain* 1983, 17:321–339.

20. Wu G, Ringkamp M, Hartke T V, Murinson BB, Campbell JN, Griffin JW, Meyer R a: Early onset of spontaneous activity in uninjured C-fiber nociceptors after injury to neighboring nerve fibers. *J Neurosci* 2001, 21:RC140.

21. Mogil J, Wilson S, Bon K, Lee S, Chung K, Raber P, Pieper J, Hain H, Belknap J, Hubert L, Elmer G, Chung J, Devor M: Heritability of nociception I: responses of 11 inbred mouse strains on 12 measures of nociception. *Pain* 1999, 80:67–82.

22. Diatchenko L, Nackley AG, Tchivileva IE, Shabalina S a, Maixner W: Genetic architecture of human pain perception. *Trends Genet* 2007, 23:605–13.

23. Costigan M, Scholz J, Woolf CJ: Neuropathic pain: a maladaptive response of the nervous system to damage. *Annu Rev Neurosci* 2009, 32:1–32.

24. Nielsen CS, Stubhaug A, Price DD, Vassend O, Czajkowski N, Harris JR: Individual differences in pain sensitivity: genetic and environmental contributions. *Pain* 2008, 136:21–9.

25. Gibbs R a, Weinstock GM, Metzker ML, Muzny DM, Sodergren EJ, Scherer S, Scott G, Steffen D, Worley KC, Burch PE, Okwuonu G, Hines S, Lewis L, DeRamo C, Delgado O, Dugan-Rocha S, Miner G, Morgan M, Hawes A, Gill R, Celera, Holt R a, Adams MD, Amanatides PG, Baden-Tillson H, Barnstead M, Chin S, Evans C a, Ferriera S, Fosler C, et al.: Genome sequence of the Brown Norway rat yields insights into mammalian evolution. *Nature* 2004, 428:493–521.

26. Doerfler W, Hoeveler A, Weisshaar B, Dobrzanski P, Knebel D, Langner KD, Achten S, Müller U: Promoter inactivation or inhibition by sequence-specific methylation and mechanisms of reactivation. *Cell Biophys* 1989, 15:21–7.

27. Ball MP, Li JB, Gao Y, Lee J-H, LeProust EM, Park I-H, Xie B, Daley GQ, Church GM: Targeted and genome-scale strategies reveal gene-body methylation signatures in

human cells. *Nat Biotechnol* 2009, 27:361–8.

28. Han H, Cortez CC, Yang X, Nichols PW, Jones P a, Liang G: DNA methylation directly silences genes with non-CpG island promoters and establishes a nucleosome occupied promoter. *Hum Mol Genet* 2011, 20:4299–310.

29. Deaton M, Webb S, Kerr ARW, Illingworth RS, Guy J, Andrews R, Bird A: Cell type – specific DNA methylation at intragenic CpG islands in the immune system. *Genome Researh* 2011, 21:1074–1086.

30. Decosterd I, Woolf CJ: Spared nerve injury: an animal model of persistent peripheral neuropathic pain. *Pain* 2000, 87:149–58.

31. Bennett G, Xie Y: A peripheral mononeuropathy in rat that produces disorders of pain sensation like those seen in man. *Pain* 1988, 33:87–107.

32. Kim SH, Chung JM: An experimental model for peripheral neuropathy produced by segmental spinal nerve ligation in the rat. *Pain* 1992, 50:355–363.

33. Hammer P, Banck MS, Amberg R, Wang C, Petznick G, Luo S, Khrebtukova I, Schroth GP, Beyerlein P, Beutler AS: mRNA-seq with agnostic splice site discovery for nervous system transcriptomics tested in chronic pain. *Genome Res* 2010, 20:847–860.

34. Heard E, Clerc P, Avner P: X-Chromosome Inactivation. *Annu Rev Genet* 1997, 31:571–610.

35. Li E, Beard C, Jaenisch R: Role for DNA methylation in genomic imprinting. *Nature* 1993, 366:362–365.

36. Feinberg AP, Vogelstein B: Hypomethylation distinguishes genes of some human cancers from their normal counterparts. *Nature* 1983, 301:89–92.

37. Jones P a, Baylin SB: The fundamental role of epigenetic events in cancer. *Nat Rev Genet* 2002, 3:415–28.

38. Song F, Mahmood S, Ghosh S, Liang P, Smiraglia DJ, Nagase H, Held W a: Tissue specific differentially methylated regions (TDMR): Changes in DNA methylation during development. *Genomics* 2009, 93:130–9.

39. Byun H-M, Siegmund KD, Pan F, Weisenberger DJ, Kanel G, Laird PW, Yang AS: Epigenetic profiling of somatic tissues from human autopsy specimens identifies tissue- and individual-specific DNA methylation patterns. *Hum Mol Genet* 2009, 18:4808–17.

40. Ghosh S, Yates AJ, Frühwald MC, Miecznikowski JC, Plass C, Smiraglia DJ: Tissue specific DNA methylation of CpG islands in normal human adult somatic tissues distinguishes neural from non-neural tissues. *Epigenetics* 2010, 5:527–538.

41. Reik W, Dean W, Walter J: Epigenetic reprogramming in mammalian development. *Science* 2001, 293:1089–93.

42. Smith ZD, Chan MM, Mikkelsen TS, Gu H, Gnirke A, Regev A, Meissner A: A unique regulatory phase of DNA methylation in the early mammalian embryo. *Nature* 2012, 484:339–344.

43. Guo JU, Ma DK, Mo H, Ball MP, Jang M-H, Bonaguidi M a, Balazer J a, Eaves HL, Xie B, Ford E, Zhang K, Ming G-L, Gao Y, Song H: Neuronal activity modifies the DNA methylation landscape in the adult brain. *Nat Neurosci* 2011, 14:1345–1351.

44. Miller C, Sweatt D: Covalent Modification of DNA Regulates Memory Formation. *Neuron* 2007, 53:857–869.

45. Wang S-C, Oelze B, Schumacher A: Age-specific epigenetic drift in late-onset Alzheimer's disease. *PLoS One* 2008, 3:e2698.

46. Lord J, Cruchaga C: The epigenetic landscape of Alzheimer's disease. *Nat Neurosci* 2014, 17:1138–1140.

47. Szulwach KE, Li X, Li Y, Song C-X, Wu H, Dai Q, Irier H, Upadhyay AK, Gearing M, Levey AI, Vasanthakumar A, Godley L a, Chang Q, Cheng X, He C, Jin P: 5-hmC-mediated epigenetic dynamics during postnatal neurodevelopment and aging. *Nat Neurosci* 2011, 14:1607–1616.

48. Heyn H, Li N, Ferreira HJ, Moran S, Pisano DG, Gomez A, Diez J, Sanchez-Mut J V., Setien F, Carmona FJ, Puca a. a., Sayols S, Pujana M a., Serra-Musach J, Iglesias-Platas I, Formiga F, Fernandez a. F, Fraga MF, Heath SC, Valencia A, Gut IG, Wang J, Esteller M: Distinct DNA methylomes of newborns and centenarians. *Proc Natl Acad Sci* 2012.

49. Gardiner-Garden M, Frommer M: CpG islands in vertebrate genomes. *J Mol Biol* 1987, 196:261–82.

50. Illingworth RS, Bird AP: CpG islands--'a rough guide'. *FEBS Lett* 2009, 583:1713–20.

51. Robinson PN, Böhme U, Lopez R, Mundlos S, Nürnberg P: Gene-Ontology analysis reveals association of tissue-specific 5' CpG-island genes with development and embryogenesis. *Hum Mol Genet* 2004, 13:1969–78.

52. Ponger L, Duret L, Mouchiroud D: Determinants of CpG Islands : Expression in Early Embryo and Isochore Structure. *Genome Res* 2001, 11:1854–1860.

53. Illingworth R, Kerr A, Desousa D, Jørgensen H, Ellis P, Stalker J, Jackson D, Clee C, Plumb R, Rogers J, Humphray S, Cox T, Langford C, Bird A: A novel CpG island set identifies tissue-specific methylation at developmental gene loci. *PLoS Biol* 2008, 6:e22.

54. Ng CW, Yildirim F, Yap YS, Dalin S, Matthews BJ, Velez PJ, Labadorf A, Housman DE, Fraenkel E: Extensive changes in DNA methylation are associated with expression of mutant huntingtin. *Proc Natl Acad Sci U S A* 2013, 110:2354–9.

55. Kim JH, Dhanasekaran SM, Prensner JR, Cao X, Robinson D, Kalyana-sundaram S, Huang C, Shankar S, Jing X, Iyer M, Hu M, Sam L, Grasso C, Maher CA, Palanisamy N, Mehra R, Kominsky HD, Siddiqui J, Yu J, Qin ZS, Chinnaiyan AM: Deep sequencing reveals distinct patterns of DNA methylation in prostate cancer. *Genome Res* 2011, 21:1028–1041.

56. Hartung T, Zhang L, Kanwar R, Khrebtukova I, Reinhardt M, Wang C, Therneau TM, Banck MS, Schroth GP, Beutler AS: Diametrically opposite methylome-transcriptome relationships in high- and low-CpG promoter genes in postmitotic neural rat tissue. *Epigenetics* 2012, 7:421–8.

57. Saxonov S, Berg P, Brutlag DL: A genome-wide analysis of CpG dinucleotides in the human genome distinguishes two distinct classes of promoters. *Proc Natl Acad Sci U S A* 2006, 103:1412–7.

58. Irizarry R a, Ladd-Acosta C, Wen B, Wu Z, Montano C, Onyango P, Cui H, Gabo K, Rongione M, Webster M, Ji H, Potash JB, Sabunciyan S, Feinberg AP: The human colon cancer methylome shows similar hypo- and hypermethylation at conserved tissue-specific CpG island shores. *Nat Genet* 2009, 41:178–86.

59. Weber M, Hellmann I, Stadler MB, Ramos L, Pääbo S, Rebhan M, Schübeler D: Distribution, silencing potential and evolutionary impact of promoter DNA methylation in the human genome. *Nat Genet* 2007, 39:457–66.

60. Doi A, Park I-H, Wen B, Murakami P, Aryee MJ, Irizarry R, Herb B, Ladd-Acosta C, Rho J, Loewer S, Miller J, Schlaeger T, Daley GQ, Feinberg AP: Differential methylation of tissue- and cancer-specific CpG island shores distinguishes human induced pluripotent stem cells, embryonic stem cells and fibroblasts. *Nat Genet* 2009, 41:1350–3.

61. Maunakea AK, Nagarajan RP, Bilenky M, Ballinger TJ, D'Souza C, Fouse SD, Johnson BE, Hong C, Nielsen C, Zhao Y, Turecki G, Delaney A, Varhol R, Thiessen N, Shchors K, Heine VM, Rowitch DH, Xing X, Fiore C, Schillebeeckx M, Jones SJM, Haussler D, Marra M a, Hirst M, Wang T, Costello JF: Conserved role of intragenic DNA methylation in regulating alternative promoters. *Nature* 2010, 466:253–7.

62. Rakyan VK, Down TA, Thorne NP, Flicek P, Kulesha E, Gräf S, Tomazou EM, Bäckdahl L, Johnson N, Herberth M, Howe KL, Jackson DK, Miretti MM, Fiegler H, Marioni JC, Birney E, Hubbard TJP, Carter NP, Tavaré S, Beck S: An integrated resource for genome-wide identification and analysis of human tissue-specific differentially methylated regions (tDMRs). *Genome Res* 2008, 18:1518–1529.

63. Brunner AL, Johnson DS, Kim SW, Valouev A, Reddy TE, Neff NF, Anton E, Medina C, Nguyen L, Chiao E, Oyolu CB, Schroth GP, Absher DM, Baker JC, Myers RM: Distinct DNA methylation patterns characterize differentiated human embryonic stem cells and developing human fetal liver. *Genome Res* 2009, 19:1044–56.

64. Meissner A, Mikkelsen TS, Gu H, Wernig M, Hanna J, Sivachenko A, Zhang X, Bernstein BE, Nusbaum C, Jaffe DB, Gnirke A, Jaenisch R, Lander ES: Genome-scale DNA methylation maps of pluripotent and differentiated cells. *Nature* 2008, 454:766–70.

65. Guo JU, Ma DK, Mo H, Ball MP, Jang M-H, Bonaguidi M a, Balazer J a, Eaves HL, Xie B, Ford E, Zhang K, Ming G, Gao Y, Song H: SI Neuronal activity modifies the DNA methylation landscape in the adult brain. *Nat Neurosci* 2011, 14:1345–51.

66. Herb BR, Wolschin F, Hansen KD, Aryee MJ, Langmead B, Irizarry R, Amdam G V, Feinberg AP: Reversible switching between epigenetic states in honeybee behavioral subcastes. *Nat Neurosci* 2012, 15:1371–1373.

67. Miller CA, Gavin CF, White JA, Parrish RR, Honasoge A, Yancey CR, Rivera IM, Rubio MD, Rumbaugh G, Sweatt JD: Cortical DNA methylation maintains remote memory. *Nat Neurosci* 2010, 13:664–666.

68. Klengel T, Mehta D, Anacker C, Rex-Haffner M, Pruessner JC, Pariante CM, Pace TWW, Mercer KB, Mayberg HS, Bradley B, Nemeroff CB, Holsboer F, Heim CM, Ressler KJ, Rein T, Binder EB: Allele-specific FKBP5 DNA demethylation mediates gene-childhood trauma interactions. *Nat Neurosci* 2013, 16:33–41.

69. Zhang Z, Cai Y-Q, Zou F, Bie B, Pan ZZ: Epigenetic suppression of GAD65

expression mediates persistent pain. *Nat Med* 2011, 17:1448–55.

70. Tajerian M, Alvarado S, Millecamps M, Dashwood T, Anderson KM, Haglund L, Ouellet J, Szyf M, Stone LS: DNA methylation of SPARC and chronic low back pain. *Mol Pain* 2011, 7:65.

71. Zhu X-Y, Huang C-S, Li Q, Chang R-M, Song Z-B, Zou W-Y, Guo Q-L: p300 exerts an epigenetic role in chronic neuropathic pain through its acetyltransferase activity in rats following chronic constriction injury (CCI). *Mol Pain* 2012, 8:84.

72. Uchida H, Matsushita Y, Ueda H: Epigenetic regulation of BDNF expression in the primary sensory neurons after peripheral nerve injury: implications in the development of neuropathic pain. *Neuroscience* 2013, 240:147–54.

73. Oki Y, Issa J-PJ: Review: Recent Clinical Trials in Epigenetic Therapy. *Rev Recent Clin Trials* 2006, 1:169–182.

74. Tajerian M, Alvarado S, Millecamps M, Vachon P, Crosby C, Bushnell MC, Szyf M, Stone LS: Peripheral nerve injury is associated with chronic, reversible changes in global DNA methylation in the mouse prefrontal cortex. *PLoS One* 2013, 8:e55259.

75. Eckhardt F, Lewin J, Cortese R, Rakyan VK, Attwood J, Burger M, Burton J, Cox T V, Davies R, Down T a, Haefliger C, Horton R, Howe K, Jackson DK, Kunde J, Koenig C, Liddle J, Niblett D, Otto T, Pettett R, Seemann S, Thompson C, West T, Rogers J, Olek A, Berlin K, Beck S: DNA methylation profiling of human chromosomes 6, 20 and 22. *Nat Genet* 2006, 38:1378–85.

76. Lister R, Pelizzola M, Dowen RH, Hawkins RD, Hon G, Tonti-Filippini J, Nery JR, Lee L, Ye Z, Ngo Q-M, Edsall L, Antosiewicz-Bourget J, Stewart R, Ruotti V, Millar a H, Thomson J a, Ren B, Ecker JR: Human DNA methylomes at base resolution show widespread epigenomic differences. Suppl mat. *Nature* 2009, 462:315–22.

77. Meissner A, Gnirke A, Bell GW, Ramsahoye B, Lander ES, Jaenisch R: Reduced representation bisulfite sequencing for comparative high-resolution DNA methylation analysis. *Nucleic Acids Res* 2005, 33:5868–77.

78. Jin S-X, Zhuang Z-Y, Woolf CJ, Ji R-R: P38 Mitogen-Activated Protein Kinase Is Activated After a Spinal Nerve Ligation in Spinal Cord Microglia and Dorsal Root Ganglion Neurons and Contributes To the Generation of Neuropathic Pain. *J Neurosci* 2003, 23:4017–22.

79. Schafers M, Sorkin L, Geis C, Shubayev V: Spinal nerve ligation induces transient upregulation of tumor necrosis factor receptors 1 and 2 in injured and adjacent uninjured dorsal root ganglia in the rat. *Neurosci Lett* 2003, 347:179–182.

80. Aldrich BT, Frakes EP, Kasuya J, Hammond DL, Kitamoto T: Changes in expression of sensory organ-specific microRNAs in rat dorsal root ganglia in association with mechanical hypersensitivity induced by spinal nerve ligation. *Neuroscience* 2009, 164:711–23.

81. LaBuda CJ, Little PJ: Pharmacological evaluation of the selective spinal nerve ligation model of neuropathic pain in the rat. *J Neurosci Methods* 2005, 144:175–81.

82. Woolf CJ, Mannion RJ: Neuropathic pain: aetiology, symptoms, mechanisms, and management. *Lancet* 1999, 353:1959–64.

83. Chung JM, Kim HK, Chung K: Segmental spinal nerve ligation model of neuropathic pain. In *Methods in Molecular Medicine*. *Volume 99*. Edited by Luo Z. Totowa, New Jersey: Humana Press; 2004:35–45.

84. Lister R, Pelizzola M, Dowen RH, Hawkins RD, Hon G, Tonti-Filippini J, Nery JR, Lee L, Ye Z, Ngo Q-M, Edsall L, Antosiewicz-Bourget J, Stewart R, Ruotti V, Millar a H, Thomson J a, Ren B, Ecker JR: Human DNA methylomes at base resolution show widespread epigenomic differences. *Nature* 2009, 462:315–22.

85. Langmead B, Trapnell C, Pop M, Salzberg SL: Ultrafast and memory-efficient alignment of short DNA sequences to the human genome. *Genome Biol* 2009, 10:R25.

86. Heinz S, Benner C, Spann N, Bertolino E, Lin YC, Laslo P, Cheng JX, Murre C, Singh H, Glass CK: Simple combinations of lineage-determining transcription factors prime cis-regulatory elements required for macrophage and B cell identities. *Mol Cell* 2010, 38:576–89.

87. Mortazavi A, Williams BA, Mccue K, Schaeffer L, Wold B: Mapping and quantifying mammalian transcriptomes by RNA-Seq. *Nat Methods* 2008, 5:1–8.

88. Emery EC, Young GT, Berrocoso EM, Chen L, McNaughton PA: HCN2 Ion Channels Play a Central Role in Inflammatory and Neuropathic Pain. *Science (80-)* 2011, 333(September):1462–1466.

89. Slater PG, Ramirez VT, Gonzalez-Billault C, Varela-Nallar L, Inestrosa NC: Frizzled-5 receptor is involved in neuronal polarity and morphogenesis of hippocampal neurons. *PLoS One* 2013, 8:e78892.

90. Boeckers TM, Bockmann J, Kreutz MR, Gundelfinger ED: ProSAP/Shank proteins - a family of higher order organizing molecules of the postsynaptic density with an emerging role in human neurological disease. *J Neurochem* 2002, 81:903–10.

91. Shcheglovitov A, Shcheglovitova O, Yazawa M, Portmann T, Shu R, Sebastiano V, Krawisz A, Froehlich W, Bernstein J a, Hallmayer JF, Dolmetsch RE: SHANK3 and IGF1 restore synaptic deficits in neurons from 22q13 deletion syndrome patients. *Nature* 2013, 503:267–71.

92. Seijffers R, Mills CD, Woolf CJ: ATF3 increases the intrinsic growth state of DRG neurons to enhance peripheral nerve regeneration. *J Neurosci* 2007, 27:7911–20.

93. Wan G, Yang K, Lim Q 'En, Zhou L, He BP, Wong HK, Too H-P: Identification and validation of reference genes for expression studies in a rat model of neuropathic pain. *Biochem Biophys Res Commun* 2010, 400:575–80.

94. Scholz J, Woolf CJ: The neuropathic pain triad: neurons, immune cells and glia. *Nat Neurosci* 2007, 10:1361–8.

95. Ben-Yaakov K, Dagan SY, Segal-Ruder Y, Shalem O, Vuppalanchi D, Willis DE, Yudin D, Rishal I, Rother F, Bader M, Blesch A, Pilpel Y, Twiss JL, Fainzilber M: Axonal transcription factors signal retrogradely in lesioned peripheral nerve. *EMBO J* 2012, 31:1350–63.

96. Jankowski MP, Cornuet PK, Mcilwrath S, Koerber HR, Albers KM: SRY-Box Containing Gene 11 (Sox11) Transcription Factor Is Required for Neuron Survival and Neurite Growth. *Neuroscience* 2006, 143:501–514.

97. Bird AP, Wolffe AP: Methylation-induced repression--belts, braces, and chromatin. *Cell* 1999, 99:451–4.

98. Kulis M, Heath S, Bibikova M, Queirós AC, Navarro A, Clot G, Martínez-Trillos A, Castellano G, Brun-Heath I, Pinyol M, Barberán-Soler S, Papasaikas P, Jares P, Beà S, Rico D, Ecker S, Rubio M, Royo R, Ho V, Klotzle B, Hernández L, Conde L, López-Guerra M, Colomer D, Villamor N, Aymerich M, Rozman M, Bayes M, Gut M, Gelpí JL, et al.: Epigenomic analysis detects widespread gene-body DNA hypomethylation in chronic lymphocytic leukemia. *Nat Genet* 2012, 44:1236–42.

99. Bacon A, Kerr NCH, Holmes FE, Gaston K, Wynick D: Characterization of an enhancer region of the galanin gene that directs expression to the dorsal root ganglion and confers responsiveness to axotomy. *J Neurosci* 2007, 27:6573–80.

100. Chen C-L, Broom DC, Liu Y, de Nooij JC, Li Z, Cen C, Samad OA, Jessell TM, Woolf CJ, Ma Q: Runx1 determines nociceptive sensory neuron phenotype and is required for thermal and neuropathic pain. *Neuron* 2006, 49:365–77.

101. Inoue K, Ozaki S, Shiga T, Ito K, Masuda T, Okado N, Iseda T, Kawaguchi S, Ogawa M, Bae S-C, Yamashita N, Itohara S, Kudo N, Ito Y: Runx3 controls the axonal projection of proprioceptive dorsal root ganglion neurons. *Nat Neurosci* 2002, 5:946–54.

102. Bergsland M, Ramsköld D, Zaouter C, Klum S, Sandberg R, Muhr J: Sequentially acting Sox transcription factors in neural lineage development. *Genes Dev* 2011, 25:2453–64.

103. Jankowski MP, McIlwrath SL, Jing X, Cornuet PK, Salerno KM, Koerber HR, Albers KM: Sox11 transcription factor modulates peripheral nerve regeneration in adult mice. *Brain Res* 2009, 1256:43–54.

104. Hu P, Mclachlan EM: Macrophage and lymphocyte invasion of dorsal root ganglia after peripheral nerve lesions in the rat. *Neuroscience* 2002, 112:23–38.

105. Lu X, Richardson PM: Responses of macrophages in rat dorsal root ganglia following peripheral nerve injury. *J Neurocytol* 1993, 22:334–41.

106. Cahoy JD, Emery B, Kaushal A, Foo LC, Zamanian JL, Christopherson KS, Xing Y, Lubischer JL, Krieg P a, Krupenko S a, Thompson WJ, Barres B a: A transcriptome database for astrocytes, neurons, and oligodendrocytes: a new resource for understanding brain development and function. *J Neurosci* 2008, 28:264–78.

107. Espina V, Wulfkuhle JD, Calvert VS, VanMeter A, Zhou W, Coukos G, Geho DH, Petricoin EF, Liotta L a: Laser-capture microdissection. *Nat Protoc* 2006, 1:586–603.

108. Eberwine J, Sul J-Y, Bartfai T, Kim J: The promise of single-cell sequencing. *Nat Methods* 2013, 11:25–27.

109. Nawy T: Single-cell sequencing. *Nat Methods* 2013, 11:18–18.

110. Wang L, Sun J, Wu H, Liu S, Wang J, Wu B, Huang S, Li N, Wang J, Zhang X: Systematic assessment of reduced representation bisulfite sequencing to human blood samples: A promising method for large-sample-scale epigenomic studies. *J Biotechnol* 2012, 157:1–6.

111. Ziller MJ, Gu H, Müller F, Donaghey J, Tsai LT-Y, Kohlbacher O, De Jager PL, Rosen ED, Bennett D a., Bernstein BE, Gnirke A, Meissner A: Charting a dynamic DNA

methylation landscape of the human genome. *Nature* 2013, 500:477–481.

112. Lam LL, Emberly E, Fraser HB, Neumann SM, Chen E, Miller GE, Kobor MS: Factors underlying variable DNA methylation in a human community cohort. *Proc Natl Acad Sci* 2012, 109:1–8.

113. Zouridis H, Deng N, Ivanova T, Zhu Y, Wong B, Huang D, Wu YH, Wu Y, Tan IB, Liem N, Gopalakrishnan V, Luo Q, Wu J, Lee M, Yong WP, Goh LK, Teh BT, Rozen S, Tan P: Methylation subtypes and large-scale epigenetic alterations in gastric cancer. *Sci Transl Med* 2012, 4:156ra140.

114. Stadler MB, Murr R, Burger L, Ivanek R, Lienert F, Schöler A, Van Nimwegen E, Wirbelauer C, Oakeley EJ, Gaidatzis D, Tiwari VK, Schübeler D: DNA-binding factors shape the mouse methylome at distal regulatory regions. *Nature* 2011, 480:490–495.

115. Kulis M, Queirós AC, Beekman R, Martín-Subero JI: Intragenic DNA methylation in transcriptional regulation, normal differentiation and cancer. *Biochim Biophys Acta* 2013, 1829:1161–74.

Eidesstattliche Versicherung

„Ich, Meike Gölzenleuchter, versichere an Eides statt durch meine eigenhändige Unterschrift, dass ich die vorgelegte Dissertation mit dem Thema: „Injury induced DNA methylome plasticity in the peripheral nervous system of the rat" selbstständig und ohne nicht offengelegte Hilfe Dritter verfasst und keine anderen als die angegebenen Quellen und Hilfsmittel genutzt habe.

Alle Stellen, die wörtlich oder dem Sinne nach auf Publikationen oder Vorträgen anderer Autoren beruhen, sind als solche in korrekter Zitierung (siehe „Uniform Requirements for Manuscripts (URM)" des ICMJE -*www.**icmje**.org*) kenntlich gemacht. Die Abschnitte zu Methodik (insbesondere praktische Arbeiten, Laborbestimmungen, statistische Aufarbeitung) und Resultaten (insbesondere Abbildungen, Graphiken und Tabellen) entsprechen den URM (s.o) und werden von mir verantwortet.

Meine Anteile an etwaigen Publikationen zu dieser Dissertation entsprechen denen, die in der untenstehenden gemeinsamen Erklärung mit dem Betreuer, angegeben sind. Sämtliche Publikationen, die aus dieser Dissertation hervorgegangen sind und bei denen ich Autor bin, entsprechen den URM (s.o) und werden von mir verantwortet.

Die Bedeutung dieser eidesstattlichen Versicherung und die strafrechtlichen Folgen einer unwahren eidesstattlichen Versicherung (§156,161 des Strafgesetzbuches) sind mir bekannt und bewusst."

Datum Unterschrift

Anteilserklärung an etwaigen erfolgten Publikationen zu dieser Dissertation

Meike Gölzenleuchter hatte folgenden Anteil an den folgender Publikation:

Meike Gölzenleuchter*, Rahul Kanwar*, Manal Zaibak, Fadi Al Saeigh, Theresa Hartung, Jana Klukas, Regenia L. Smalley, Julie M. Cunningham, Maria E. Figueroa, Gary P. Schroth, Terry M. Therneau, Michaela S. Banck, Andreas S. Beutler

* These authors contributed equally to this work

Plasticity of DNA methylation in a nerve injury model of pain, manuscript accepted for publication in *Epigenetics* (05.01.2015)

Beitrag an der Aufstellung des experimentellen Designs, den Laborexperimenten, der Analyse, der Grafikgestaltung, der Auswertung und dem Schreiben des Artikels.

Unterschrift, Datum und Stempel des betreuenden Hochschullehrers

Unterschrift der Doktorandin

Lebenslauf

Mein Lebenslauf wird aus datenschutzrechtlichen Gründen in der elektronischen Version meiner Arbeit nicht veröffentlicht

Komplette Publikationsliste

Meike Gölzenleuchter*, Rahul Kanwar*, Manal Zaibak, Fadi Al Saeigh, Theresa Hartung, Jana Klukas, Regenia L. Smalley, Julie M. Cunningham, Maria E. Figueroa, Gary P. Schroth, Terry M. Therneau, Michaela S. Banck, Andreas S. Beutler

* These authors contributed equally to this work

Plasticity of DNA methylation in a nerve injury model of pain, *Epigenetics.* 2015;10(3):200-12

Stefan K. Schulze*, Rahul Kanwar*, Meike Gölzenleuchter*, Terry M. Therneau, Andreas S. Beutler

* These authors contributed equally to this work

SERE: Single-parameter quality control and sample comparison for RNA-Seq, *BMC Genomics*. 2012;13:524

Gölzenleuchter M., Kees M.G., Hilpert J., Gramm H.J., Reich C.A

Accuracy of continuous and noninvasive total hemoglobin measurement using multiwave length pulse-oximetry in ICU patients: 3AP1-1, *Eur J Anaesthesiol.* 28():25-26, June 2011

Danksagung

Alle Experimente wurden an der Mayo Clinic, Rochester MN im Labor von Dr. Andreas Beutler durchgeführt. Mein Dank gilt daher insbesondere ihm, da er die Realisierung dieses Projekts ermöglicht hat. Ich danke Dr. Beutler für die Aufnahme in sein Labor, sein Vertrauen und die exzellente Betreuung, die ich in seiner Arbeitsgruppe erfahren durfte: Mit seinem Enthusiasmus hat er meine Freude am wissenschaftlichen Arbeiten geweckt.

Rahul Kanwar danke ich für seine Geduld während der Einarbeitungsphase, die vielfältigen interessanten Diskussionen, sowie die enge Zusammenarbeit während des gesamten Projekts.

Bei Prof. Therneau möchte ich mich für seine große Hilfsbereitschaft und die wertvollen Gespräche über Statistik bedanken.

Prof. Dr. Meisel danke ich für seine Unterstützung und sein großartiges Engagement.

Bei Manal Zaibak möchte ich mich für die fröhliche Zusammenarbeit bei den Tierexperimenten und die tollen Unternehmungen bedanken, die zu der Entstehung einer wahren Freundschaft geführt haben. Bei Fadi Al-Saeigh bedanke ich mich für die Durchführung der Tierexperimente, welche die RNA-Seq Daten generiert haben, die in der vorliegenden Arbeit für die Methylom-Transkriptom-Analyse genutzt wurden. Ich danke Stefan Schulze für die Einarbeitung in das Grafikprogramm, die motivierenden Gespräche und die zahlreichen Tipps. Bei Amit Kulkarni, Jana Klukas, Rahul Kanwar, Ganesh Boora, Stefan Schulze, Manal Zaibak, Kay Minn, Josef Pleticha, Franziska Metge, Theresa Hartung und Christian Singh bedanke ich mich für all die lustigen Momente in unserem Büro, im Labor oder außerhalb der Klinik.

Außerdem bedanke ich mich ganz herzlich bei Prof. Stolte, Leiter des „Biomedical Exchange Programms“, der meinen Aufenthalt in den USA überhaupt erst ermöglicht hat.

Abschließend möchte ich meinen Eltern und Freunden danken, die mich während der gesamten Dauer des Projekts unterstützt und ermutigt haben.